

1 **Measurement report: Atmospheric nitrate radical chemistry in the**
2 **South China Sea influenced by the urban outflow of the Pearl River**
3 **Delta**

4 Jie Wang^{1,2}, Haichao Wang^{1,2*}, Yee Jun Tham^{3,4*}, Lili Ming⁵, Zelong Zheng¹, Guizhen
5 Fang³, Cuizhi Sun^{1,2}, Zhenhao Ling^{1,2}, Jun Zhao^{1,2}, Shaojia Fan^{1,2}

6 ¹ School of Atmospheric Sciences, Sun Yat-sen University, and Southern Marine Science
7 and Engineering Guangdong Laboratory (Zhuhai), Zhuhai, 519082, China

8 ² Guangdong Provincial Observation and Research Station for Climate Environment and
9 Air Quality Change in the Pearl River Estuary, Key Laboratory of Tropical Atmosphere-
10 Ocean System (Sun Yat-sen University), Ministry of Education, Zhuhai, 519082, China

11 ³ School of Marine Sciences, Sun Yat-sen University, Zhuhai 519082, China.

12 ⁴ Pearl River Estuary Marine Ecosystem Research Station, Ministry of Education, Zhuhai,
13 519082, China.

14 ⁵ Technical Center of Gongbei Customs District of China, Zhuhai, 519000, China.

15

16 *Correspondence to:* Haichao Wang (wanghch27@mail.sysu.edu.cn); Yee Jun Tham
17 (thamyj@mail.sysu.edu.cn)

18

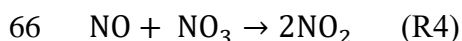
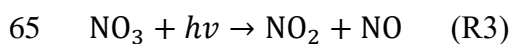
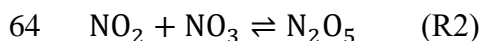
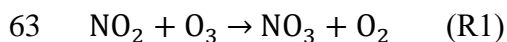
19 **Abstract.** Nitrate radical (NO₃) is a critical nocturnal atmospheric oxidant in the
20 troposphere, which widely affects the fate of air pollutants and regulates air quality. Many
21 previous works have reported the chemistry of NO₃ in inland regions of China, while ~~less~~
22 ~~study targets fewer studies target~~ marine regions. Here, we present a field measurement of
23 the NO₃ reservoir, dinitrogen pentoxide (N₂O₅), and related species at a typical marine site
24 (Da Wan Shan Island) located in the South China Sea in the winter of 2021. Two patterns
25 of air masses were captured during the campaign, including the dominant airmass from
26 inland China (IAM) with a percentage of ~84%, and the airmass from eastern coastal areas
27 (CAM) with ~16%. During the IAM period, the NO₃ production rate reached 1.6 ± 0.9
28 ppbv h⁻¹ due to the transportation of the polluted urban plume with high NO_x and O₃. While
29 the average nocturnal N₂O₅ and the calculated NO₃ mixing ratio were 119.5 ± 128.6 pptv
30 and 9.9 ± 12.5 pptv, respectively, and the steady state lifetime of NO₃ was 0.5 ± 0.7 min on
31 average, indicating intensive nighttime chemistry and rapid NO₃ loss at this site. By
32 examining the reaction of NO₃ with volatile organic compounds (VOCs) and N₂O₅
33 heterogeneous hydrolysis, we revealed that these two reaction pathways were not
34 responsible for the NO₃ loss (<20%), since the NO₃ reactivity (k(NO₃)) towards VOCs was

35 small ($5.2 \times 10^{-3} \text{ s}^{-1}$) and the aerosol loading was low. Instead, NO was proposed to
36 significantly contribute to nocturnal NO_3 loss at this site, despite the nocturnal NO
37 concentration always at sub-ppbv level and near the instrument detection limit. It might be
38 from the local soil emission or others. We infer that the nocturnal chemical NO_3 reactions
39 would be largely enhanced once without NO emission in the open ocean after the air mass
40 passes through this site, thus highlighting the strong influences of the urban outflow to the
41 downwarddownwind marine areas in terms of nighttime chemistry. During the CAM period,
42 nocturnal ozone was higher, while NO_x was much lower. The NO_3 production was still very
43 fast, with a rate of 1.2 ppbv h^{-1} . With the absence of N_2O_5 measurement in this period, the
44 NO_3 reactivity towards VOCs and N_2O_5 uptake were calculated to assess NO_3 loss
45 processes. We showed that the average $k(\text{NO}_3)$ from VOCs (56.5%, $2.6 \pm 0.9 \times 10^{-3} \text{ s}^{-1}$)
46 was higher than that from N_2O_5 uptake (43.5%, $2.0 \pm 1.5 \times 10^{-3} \text{ s}^{-1}$) during the CAM period,
47 indicating a longer $\text{NO}_3/\text{N}_2\text{O}_5$ lifetime than that during IAM period. This study improves
48 the understanding of the nocturnal NO_3 budget and environmental impacts with the
49 interaction of anthropogenic and natural activities in marine regions.

50

51 1. Introduction

52 Reactive nitrogen compounds, especially the nitrate radical (NO_3) and dinitrogen pentoxide
53 (N_2O_5) play an essential role in nocturnal atmospheric chemistry (Wayne et al., 1991;
54 Brown and Stutz, 2012). NO_3 is mainly generated via the oxidation of NO_2 by O_3 (R1), and
55 then NO_3 further reacts with NO_2 to produce N_2O_5 (R2) with a thermal equilibrium. The
56 temperature-dependent equilibrium constant, K_{eq} , regulates the equilibrium favoring NO_3
57 and NO_2 at higher temperatures (Osthoff et al., 2007; Chen et al., 2022). During daytime,
58 the NO_3 mixing ratio is generally low as its lifetime is very short ($< 5 \text{ s}$) due to the fast
59 photolysis (R3) and rapid reaction with NO (R4) (a rate constant of $2.6 \times 10^{-11} \text{ cm}^3$
60 $\text{molecule}^{-1} \text{ s}^{-1}$ at 298 K; Atkinson et al., 2004). While at night, NO_3 accumulates and can
61 reach tens to hundreds of parts per trillion by volume (pptv), making it the major nocturnal
62 oxidizing agent (Wang et al., 2015).



67 During nighttime, NO₃ is the most important oxidant for alkenes (Mogensen et al., 2015;
68 Edwards et al., 2017), particularly in rural, remote, or forested environments, where it
69 predominantly reacts with unsaturated biogenic volatile organic compounds (VOCs),
70 especially isoprene and monoterpene (Ng et al., 2017; Liebmann et al., 2018b; Liebmann
71 et al., 2018a), to form alkyl nitrates (RONO₂), that ultimately lead to secondary organic
72 aerosols (SOAs) (Brown and Stutz, 2012). The observations and model simulations showed
73 that the measured particulate organic nitrates were largely attributed to the nocturnal NO₃
74 oxidation across Europe (Kiendler-Scharr et al., 2016). The NO₃ oxidation was also
75 reported to play an important role in aerosol formation in the Southeastern United States
76 with high isoprene and monoterpene emissions (Xu et al., 2015). These studies highlighted
77 the critical role of the reaction of NO₃ with VOCs in NO₃ budget and organic aerosol
78 pollution. In addition, NO₃ also reacts with dimethyl sulfide (DMS) over the ocean,
79 affecting the marine sulfur cycle and thus cloud formation and global climate (Aldener et
80 al., 2006; Brown and Stutz, 2012; Ian Barnes et al., 2006; Rosati et al., 2022). While in
81 high aerosol loading regimes, the N₂O₅ heterogeneous uptake becomes a significant
82 indirect NO₃ loss pathway. The hydrolysis reaction produces nitrate (NO₃⁻) and nitryl
83 chloride (ClNO₂) on chloride-containing ~~aerosols~~aerosol surfaces (Osthoff et al., 2008;
84 Thornton et al., 2010), in which ClNO₂ activates the Cl radical and further enhances the
85 photochemistry and ozone pollution in the following day (Riedel et al., 2012; Riedel et al.,
86 2014; Behnke et al., 1993).

87 Different NO₃ loss pathways produce different air pollutants ~~and cause different~~
88 ~~environmental impacts, thus~~ characterization of NO₃ budget is essential to clarify the NO₃
89 chemistry in air pollution under various environments. Observations of N₂O₅ and NO₃ in
90 different regions and evaluation of their loss processes have been reported in numerous
91 studies (Crowley et al., 2011; Geyer et al., 2001; Brown et al., 2011; Dewald et al., 2022;
92 Niu et al., 2022; Brown et al., 2016; Wang et al., 2020a; Tham et al., 2016; Aldener et al.,
93 2006; Lin et al., 2022). In general, the NO₃ loss process shows significant regional
94 differences. In urban areas featuring intensive anthropogenic NO_x emissions and moderate
95 (or high) aerosol loading, N₂O₅ uptake is comparable or even dominates the NO₃ loss
96 (Wang et al., 2013). While in rural and forested areas with abundant biogenic ~~VOCs~~VOC
97 (BVOC) emissions, the NO₃ loss processes were usually dominated by BVOCs (Dewald
98 et al., 2022; Geyer et al., 2001; Brown et al., 2011). As for the coastal areas, which were
99 jointly affected by the polluted air mass from the inland and the relatively clean air mass
100 from the ocean, the dominant NO₃ loss process varies greatly depending on the air mass
101 origin (Aldener et al., 2006; Niu et al., 2022; Brown et al., 2016; Crowley et al., 2011). For
102 instance, Crowley et al. (2011) found in the Atlantic coast of Southern Spain (forested area)
103 that when the air mass mainly originated from the Atlantic, NO₃ was mainly consumed by
104 BVOCs (mainly monoterpenes) emitted from nearby forests, while when the air mass came

105 from the continent, NO₃ loss was mainly due to reactions with anthropogenic VOCs
106 (AVOCs).

107 China has been recently proven to be a hot spot of nocturnal chemistry with a high NO₃
108 production rate (Wang et al., 2023). Many studies have reported the mechanisms, budget,
109 or impacts of NO₃-N₂O₅ chemistry in different regions, while most of them were conducted
110 in urban regions (Wang et al., 2013; Yan et al., 2021; Wang et al., 2020a; Wang et al., 2017c;
111 Wang et al., 2017d). For example, Wang et al. (2017b) showed a significant contribution
112 of N₂O₅ uptake to nitrate pollution in summer and winter, and they also highlighted the fast
113 organic nitrate production rate observed in Beijing rural region in summer (Wang et al.,
114 2018b). Only several studies focused on nighttime oxidation in coastal cities like Shanghai,
115 Shenzhen, and Hong Kong (Zhu et al., 2022; Niu et al., 2022; Yan et al., 2019), which
116 showed different patterns of NO₃ chemistry compared with urban regions. Even fewer field
117 studies were conducted on the island which is far away from the coastal cities where the
118 interactions of the oceanic atmosphere and urban plumes can significantly affect the NO₃
119 budget and impacts. Given the diversity of air masses in inland and coastal areas, studies
120 are needed to gain a comprehensive understanding of NO₃ losses in different atmospheric
121 environments, particularly in coastal and marine areas.

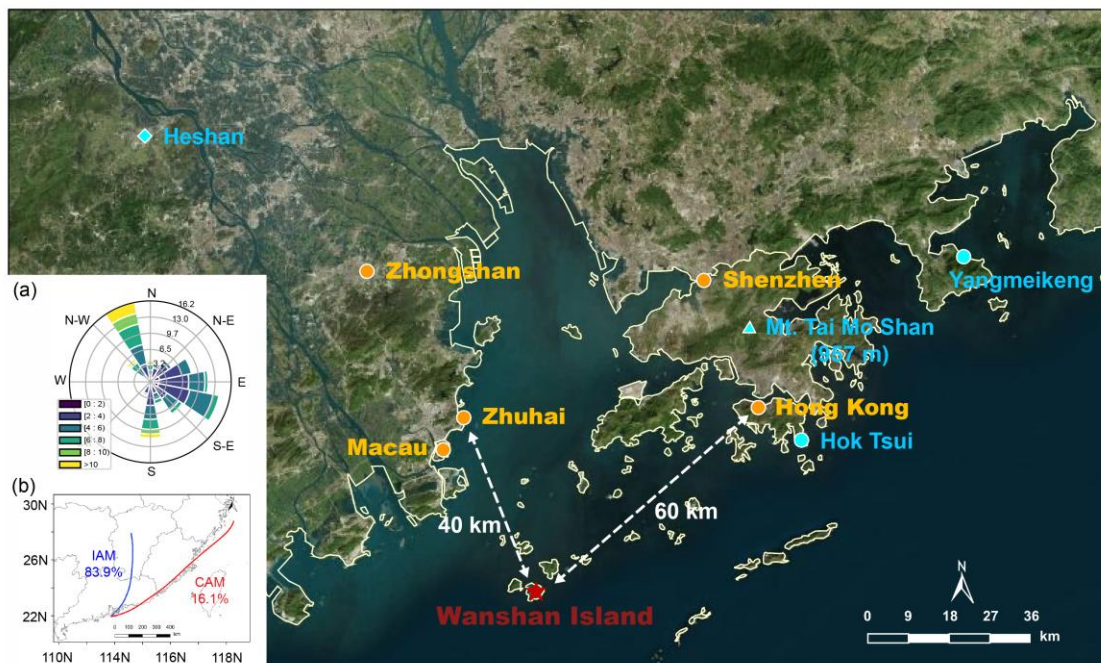
122 Therefore, we conducted an intensive field observation on Da Wan Shan Island (DWS) in
123 the winter of 2021, which is a typical island site in the north of the South China Sea, and
124 ~~downward~~downwind of the city clusters in the Pearl River Delta, China during the winter
125 monsoon periods. The island features a subtropical oceanic monsoon climate, and the north
126 and northeast synoptic winds from inland PRD and eastern China coast are generally
127 predominant in winter (Liu et al., 2019; Wang et al., 2018a). This allows us to further
128 investigate the interactions between anthropogenic emissions and marine emissions from
129 the perspective of nighttime chemistry. In this study, the measurements of N₂O₅ and the
130 related species ~~observed~~ during the DWS winter campaign are reported. We have identified
131 two types of air masses from both mainland China and coastal areas. Finally, the NO₃
132 budget and loss processes in different air masses are characterized.

133 2. Methods

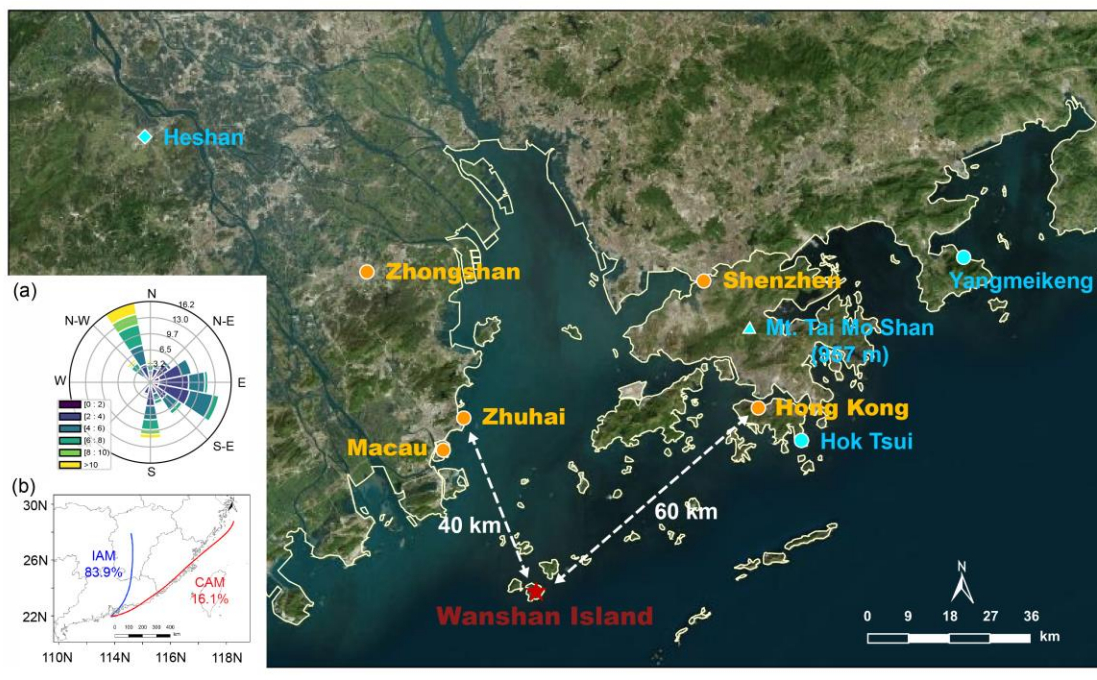
134 2.1 Site description

135 The field campaign was conducted at Da Wan Shan Island (21.~~93~~93°55'57" N,
136 113.~~72~~72°43'15" E) from Nov. 9th to Dec. 16th, 2021. Fig. 1 shows the location of the study
137 site, which is approximately 60 km southwest of Hong Kong; 40 km southeast of Zhuhai;
138 and about 100 km and 80 km away from the megacities Guangzhou and Shenzhen,

139 respectively. This island is dominated by mountainous terrain with an area of 8.1 km² and
 140 has a small population of about ~~3000~~3,000. Anthropogenic emissions are sparse and no
 141 industrial pollution sources were identified, though numerous ships engaging in local
 142 fishing activities were observed, potentially affecting the local atmosphere. During the
 143 measurement, local airflow was ~~consistent~~consistently from ~~either~~ the northwest ~~to~~
 144 southeast (Fig. 1a) due to the winter monsoon, with wind speeds most frequently ranging
 145 from 1.8 to 7.9 m s⁻¹ (10th - 90th percentiles) and an average of 4.5 ± 2.6 m s⁻¹. This wind
 146 direction is indicative of the mixing of air masses from both continental and coastal areas.
 147 The HYbrid Single-Particle Lagrangian Integrated Trajectory model (HYSPLIT) was
 148 adopted to investigate the historical trajectory. The HYSPLIT model was run for 48 hours
 149 backward in time at local times of 20:00, 24:00, and 04:00, and at a height of 70 m above
 150 sea level. It confirmed that the air mass during nighttime mostly came from
 151 ~~continental~~inland China (~~defined as inland air mass~~fresh urban emissions, IAM, 84%) and
 152 the coastal areas (~~defined as coastal air mass~~aged urban emissions, CAM, 16%). IAM
 153 featured the outflow from inland China, such as Guangzhou and Changsha, while CAM
 154 featured the outflow of coastal cities like Hong Kong and Shenzhen. No air masses free of
 155 pollution from the South China Sea were observed during the measurement period. All
 156 measurement instruments were placed in the DWS Atmospheric-Marine Research Station,
 157 located on the rooftop with inlets approximately 10 m above ground level and about 72 m
 158 above sea level. All times were given in CNST (Chinese National Standard Time = UTC +
 159 8 h), with sunrise around 06:40 CNST and sunset at 17:40 CNST.



160



161

162 **Figure 1.** A map of the field measurement site of Wanshan Island (red star) and the
 163 surrounding environment (extracted from BingSatelliteMap). Two coastal sites Hok Tsui
 164 (Yan et al., 2019) and Yangmeikeng (Niu et al., 2022), and an urban site Heshan (Wang et
 165 al., 2022; Yun et al., 2018b) are denoted as blue circle and diamond, respectively. The blue
 166 triangle denoted Mt. Tai Mo Shan (957 m), a mountainous site that studied the nighttime
 167 chemistry in the nocturnal residual layer (Brown et al., 2016). The inset plot (a) provides
 168 the wind rose for the sampling site during the campaign. Panel (b) shows the clustering
 169 result of the 48-hrs backward trajectory calculations at nighttime using the HYSPLIT
 170 model throughout the campaign.

171 2.2 Instrument setup

172 Various parameters were measured in this study, including N_2O_5 , NO, NO_2 , O_3 , VOCs,
 173 particle number size distribution (PNSD), and meteorological parameters with different
 174 instruments. The detail information about these instruments is listed in Table 1. The N_2O_5
 175 measurements were performed using a cavity-enhanced absorption spectrometer (CEAS)
 176 which has been deployed in several field campaigns (Wang et al., 2017a; Wang et al., 2017b;
 177 Wang et al., 2018b; Wang et al., 2020b). In brief, ambient N_2O_5 was thermally decomposed
 178 to NO_3 in a perfluoro alkoxy alkane (PFA) tube (length: 35 cm, I.D.: 4.35 mm) heated to
 179 $130\text{ }^\circ\text{C}$, and NO_3 was detected within a $110\text{ }^\circ\text{C}$ PFA resonator cavity. NO was injected to
 180 destroy NO_3 from N_2O_5 thermal decomposition every 5 min cycle, and the result was used
 181 as the reference spectrum to avoid the influence of ambient water vapor. A pair of high-

182 reflectivity (HR) mirrors (Layertec GmbH, Mellingen, Germany) with a diameter of 25.0
183 mm (C0.00/-0.10 mm) was used to enhance the effective optical pathlength. Mirror
184 reflectivity ($R(\lambda)$) was calibrated with high purity He and N_2 in the current experimental setup
185 during the field measurements. $R(\lambda)$ was calibrated to be 0.99997, and the effective pathlength
186 of the optical resonator was 13.96 km. A Teflon polytetrafluoroethylene (PTFE) filter was
187 used to remove ambient aerosol particles, and the inlet flow rate was $1.0 \text{ L}\cdot\text{min}^{-1}$. The loss
188 of N_2O_5 in the sampling line and filter was considered in the data correction: according to
189 previous work (Wang et al., 2017a). Here the CEAS measurement encompasses the
190 combined concentration of ambient [$N_2O_5 + NO_3$] and effectively represents N_2O_5 under high
191 NO_x (or low temperature) conditions when the NO_3 -to- N_2O_5 ratio is likely to be low.
192 Accounting for the instrument's transmission efficiency and the thermal transformation
193 between NO_3 and N_2O_5 , the contribution of NO_3 is sufficiently negligible in comparison to
194 N_2O_5 . Nevertheless, we have taken it into account during the N_2O_5 data correction. The
195 limit of detection (LOD) was 2.7 pptv (1σ), and the measurement uncertainty was $\pm 19\%$.

196

197 **Table 1.** The information of observation instruments used during the DWS campaign.

Species	Techniques	Detection limit	Accuracy	Time resolution
N ₂ O ₅	CEAS	2.7 pptv (1σ)	± 19%	10 s
NO	Chemiluminescence	0.4 ppbv	± 5%	1 min
NO ₂	Chemiluminescence	0.4 ppbv	± 5%	1 min
O ₃	UV photometry	0.4 ppbv	± 5%	1 min
VOCs	PTR-TOF-MS	0.01 ppbv	± 10%	10 s
PNSD	SMPS	5–300 nm	± 10%	5 min

198 NO_x and O₃ were measured by commercial instruments (model T200U and model T400U,
 199 Teledyne API Inc., respectively) calibrated with zero air before the measurement. The
 200 nitrogen oxide analyzer uses the chemiluminescence detection method to measure the
 201 original NO and converted NO₂, and the LOD was 0.4 ppbv for each species. Aerosol
 202 surface area density (S_a, μm² cm⁻³) was calculated based on the particle numbers and
 203 geometric diameter, which was ~~measured by a laboratory-assembled scanning-mobility~~
 204 ~~particle sizer (SMPS).~~ calculated through the results measured by a laboratory-assembled
 205 scanning-mobility particle sizer (SMPS) according to McMurry et al. (2000). This SMPS
 206 system consists of two differential mobility analyzers (DMA, "nano-DMA" mode 3081A,
 207 and "regular-DMA" mode 3085A, TSI Inc.) in parallel, and a condensed particle counter
 208 (mode 3787, TSI Inc.) as the detector. The combination of nano DMA and conventional
 209 mode 3085A DMA enables the SMPS to have better detection performance for particles
 210 below 50 nm. In this measurement, SMPS measured the particle size distribution in 5-300
 211 nm with a time resolution of 5 minutes, and S_a can be regarded as the lower limit value. A
 212 growth factor $f(\text{RH}) = 1 + 8.8 \times (\text{RH}/100)^{9.7}$ (Liu et al., 2013) was used here to correct dry
 213 state S_a to wet state S_a.

214 VOCs were measured by proton transfer reaction time of flight mass spectrometry (PTR-
 215 TOF-MS, Ionicon Analytik GmbH, Innsbruck, Austria) with a time resolution of 10 s.
 216 ~~Meanwhile, VOCs were also sampled every 2 h using 2 L canisters on the selected days~~
 217 ~~when the hourly O₃ mixing ratio exceeded 70 ppbv, and the canister samples were~~
 218 At the end of this campaign, background measurements and instrument calibration were
 219 conducted with high-purity nitrogen and multi-component VOC gas standards, respectively.
 220 The instrument calibration results yielded strong linear relationships (R² = 0.98) between
 221 the proton transfer reaction rate constants and the sensitivities of ten calibrants, including
 222 acetaldehyde, acetone, dimethyl sulfide, isoprene, methyl ethyl ketone, benzene, toluene,
 223 styrene, o-xylene, and trimethylbenzene. The sensitivities of the uncalibrated species were
 224 determined through the rate constants of the proton transfer reactions and their correlation
 225 coefficients with sensitivity. Meanwhile, the VOCs were also sampled by canister and
 226 analyzed by a gas chromatograph equipped with a mass spectrometer or flame ionization

227 detector (GC-MS) for some ozone polluted days. For the absence of nocturnal data from
 228 canister samples, the following analysis was based on the PTR-TOF-MS measurement
 229 except the weight of α -pinene and β -pinene detected by GC-MS. Since monoterpene
 230 species cannot be distinguished by PRT-TOF-MS, the reaction rate constant of the sum
 231 monoterpene reaction with NO_3 was weighted by the campaign-averaged percentage weight
 232 of α -pinene and β -pinene detected by GC-MS. Meteorological parameters (i.e.,
 233 temperature (T), relative humidity (RH), wind speed, and wind direction) were routinely
 234 monitored with a time resolution of 5 min.

235 2.3 The calculation of NO_3 budget and lifetime

236 With the observation of N_2O_5 , NO_3 can be calculated according to their temperature-
 237 dependent equilibrium relationship (Eq. 1) (Brown and Stutz, 2012). Lifetimes are
 238 commonly expressed as the ratio of their concentrations to the NO_3 production rate as
 239 determined by Eq. 2 and Eq. 3, assuming the production and loss are in dynamic balance
 240 at night (Brown et al., 2003; Brown and Stutz, 2012). The production rate of nitrate radical,
 241 $\text{P}(\text{NO}_3)$, is commonly expressed by Eq. 24, where $k_{\text{NO}_2+\text{O}_3}$ represents the temperature-
 242 dependent reaction rate constant of NO_2 and O_3 (Atkinson et al., 2004). In general, the
 243 nocturnal NO_3 losses typically include three main pathways: (Eq. 5): (1) the reaction with
 244 NO , (2) the reactions with VOCs, and (3) N_2O_5 uptake.

$$245 \quad [\text{NO}_3] = [\text{N}_2\text{O}_5] / \text{Keq}(T) [\text{NO}_2] \quad \text{_____}$$

$$246 \quad \text{Keq} = 5.50 \times 10^{-27} \times \exp(10724/T) \quad \text{_(Eq. 1)}$$

$$247 \quad \tau_{\text{N}_2\text{O}_5} = \frac{[\text{N}_2\text{O}_5]}{\text{P}(\text{NO}_3)} = \frac{[\text{N}_2\text{O}_5]}{k_{\text{NO}_2+\text{O}_3} [\text{NO}_2] [\text{O}_3]} \quad \text{(Eq. 2)}$$

$$248 \quad \tau_{\text{NO}_3} = \frac{[\text{NO}_3]}{\text{P}(\text{NO}_3)} = \frac{[\text{NO}_3]}{k_{\text{NO}_2+\text{O}_3} [\text{NO}_2] [\text{O}_3]} \quad \text{(Eq. 23)}$$

$$249 \quad \text{P}(\text{NO}_3) = k_{\text{NO}_2+\text{O}_3} [\text{O}_3] [\text{NO}_2] \quad \text{(Eq. 4)}$$

$$250 \quad \text{L}(\text{NO}_3) = \sum k_i [\text{VOC}_i] [\text{NO}_3] + k_{\text{NO}+\text{NO}_3} [\text{NO}] [\text{NO}_3] + k_{\text{het}} [\text{N}_2\text{O}_5] \quad \text{(Eq. 35)}$$

251 The NO_3 reactivity towards VOCs, $k(\text{NO}_3)$, is the first-order loss rate coefficient
 252 calculated from the products of the bimolecular rate coefficients k_i and the VOC
 253 concentrations as shown in Eq. 46.

254 $k(\text{NO}_3) = \sum k_i[\text{VOC}_i]$ (Eq. 46)

255 The k_{het} is the first-order loss rate coefficient of N_2O_5 uptake on the aerosol surface. It
 256 depends on the uptake coefficient $\gamma(\text{N}_2\text{O}_5)$, the aerosol surface area density S_a ($\mu\text{m}^2 \text{cm}^{-3}$),
 257 and the mean molecular speed c (Eq. 57). The $\gamma(\text{N}_2\text{O}_5)$ is influenced by chemical
 258 composition, physical properties of aerosol, as well as ambient conditions including related
 259 humidity and temperature (Yu et al., 2020; Wagner et al., 2013; Wang et al., 2018b; Bertram
 260 and Thornton, 2009; Tang et al., 2014; Kane et al., 2001). ~~Here $\gamma(\text{N}_2\text{O}_5)$ is parameterized~~
 261 ~~based on RH and temperature (Eq. 6). There are several kinds of methods proposed to~~
 262 ~~quantify or estimate $\gamma(\text{N}_2\text{O}_5)$ by using observed parameters. Given that some essential~~
 263 ~~parameters were not directly measured during this campaign, only two approaches were~~
 264 ~~employed to estimate the N_2O_5 uptake coefficient. The first method is the pseudo steady~~
 265 ~~state method by assuming that N_2O_5 and NO_3 have achieved a steady state (Brown et al.,~~
 266 ~~2009). $\gamma(\text{N}_2\text{O}_5)$ and k_{NO_3} can be determined from the slope and intercept of linear~~
 267 ~~regression of $K_{eq}[\text{NO}_2] \tau(\text{N}_2\text{O}_5)^{-1}$ versus $0.25cS_aK_{eq}[\text{NO}_2]$ respectively as shown in Eq.~~
 268 ~~8. The second is the parameterization method. As the aerosol compositions used to estimate~~
 269 ~~the N_2O_5 uptake coefficients were not measured, only a simplified parameterization is~~
 270 ~~available that based on relative humidity (RH) and temperature (Eq. 9) (Hallquist et al.,~~
 271 ~~2003; Kane et al., 2001; Evans and Jacob, 2005). Although simple, it had an overall~~
 272 ~~reasonable performance in China (Wang et al., 2022; Tham et al., 2018; Wang et al., 2020a).~~

273 $k_{het} = \frac{1}{4}cS_a\gamma(\text{N}_2\text{O}_5)$ (Eq. 57)

274 $K_{eq}[\text{NO}_2]\tau(\text{N}_2\text{O}_5)^{-1} = \frac{1}{4}cS_a\gamma(\text{N}_2\text{O}_5)K_{eq}[\text{NO}_2] + k_{\text{NO}_3}$ (Eq. 8)

275 $\gamma(\text{N}_2\text{O}_5) = \alpha \times 10^\beta$

276 $\alpha = 2.79 \times 10^{-4} + 1.3 \times 10^{-4} \times \text{RH} - 3.43 \times 10^{-6} \times \text{RH}^2 + 7.52 \times 10^{-8} \times \text{RH}^3$

277 $\beta = 4 \times 10^{-2} \times (T - 294)$ ($T > 282\text{K}$)

278 $\beta = -0.48$ ($T < 282\text{K}$) (Eq. 6)

279 ~~Lifetimes are commonly expressed as the ratio of their concentrations to the NO_3~~
 280 ~~production rate as determined by Eq. (7) and Eq. (8), assuming the production and loss are~~
 281 ~~in dynamic balance at night (Brown et al., 2003; Brown and Stutz, 2012).~~

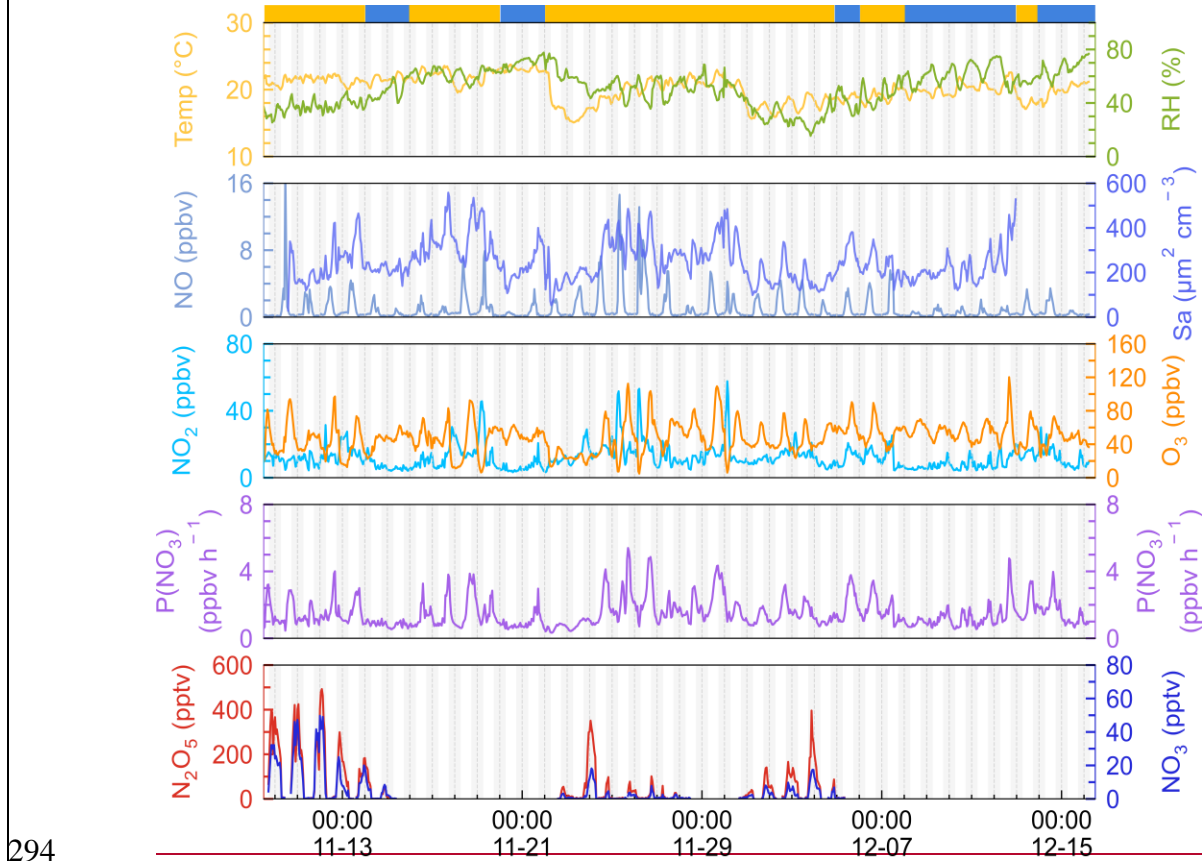
282 $\tau_{N_2O_5} = \frac{[N_2O_5]}{P(NO_3)} = \frac{[N_2O_5]}{k_{NO_2+O_3}[NO_2][O_3]} \quad (\text{Eq. 7})$

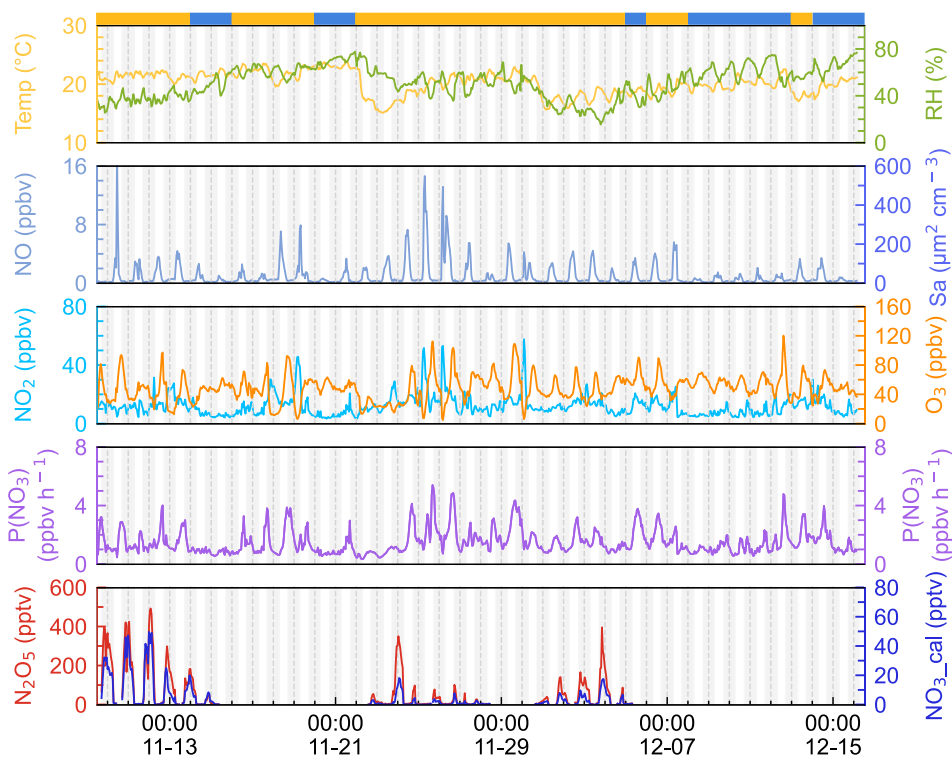
283 $\tau_{NO_3} = \frac{[NO_3]}{P(NO_3)} = \frac{[NO_3]}{k_{NO_2+O_3}[NO_2][O_3]} \quad (\text{Eq. 8})$

284 **3. Results and discussion**

285 **3.1 Measurement overview**

286 The time series of N_2O_5 , related trace gases, and selected meteorological parameters for
 287 the study period are depicted in Fig. 2. The air masses are categorized into IAM and CAM
 288 according to the backward trajectories at 20:00, 00:00, and 04:00 each day as illustrated in
 289 Fig. 1. The detailed information of two kinds of air masses is listed in Table 2. Data gaps
 290 for N_2O_5 were caused by technical problems, mirror reflectivity calibration, or instrumental
 291 maintenance, which usually took place in the daytime. In this campaign, meteorological
 292 conditions featured a typical subtropical winter climate with average temperature and RH
 293 values of $20.1 \pm 1.9 \text{ }^\circ\text{C}$ and $52.0\% \pm 13.6\%$, respectively.





295

296 **Figure 2.** Time series of N_2O_5 , NO_3 , $P(NO_3)$, NO , NO_2 , Sa , temperature, and relative
 297 humidity in 1-hour average. NO_3 was calculated by measured N_2O_5 according to the
 298 thermal equilibrium. The light gray shadow indicates the nighttime period. The ribbon at
 299 the top separates the air masses into two categories, yellow for inland air masses (IAM)
 300 and blue for coastal air masses (CAM).

301 Ozone exhibited the characteristic of afternoon photochemical peaks especially when the
 302 air mass comes from the inland. The average and maximum concentrations of ozone were
 303 48.2 ± 18.2 ppbv and 120.1 ppbv, respectively, among which. Once the hourly maximum
 304 hourly average O_3 exceeded the Chinese national air quality standard ($200 \mu g m^{-3}$,
 305 equivalent to 93 ppbv) for), we marked this day as an O_3 pollution day. There are 6 O_3
 306 polluted days out of 37 days of measurements. All these O_3 pollution episode days during
 307 the campaign and all occurred during the IAM period periods. Meanwhile, the mixing ratio
 308 of NO , NO_2 , and Sa usually increased during these days, indicating that this site was
 309 strongly affected by regional transport from inland China, i.e., the PRD region city clusters.
 310 Previous observations by Wang et al. (2018a) also found high O_3 levels in autumn on the
 311 same island due to the weak NO titration and high O_3 production rate. Detailed analysis of
 312 ozone and VOCs will be subjected to another manuscript (Fang et al., 2023).

313 Nitrogen oxides ($NO_x = NO + NO_2$) were at a moderate level with an average value of 13.1
 314 ± 8.2 ppbv, which is much lower than the values in PRD regions (usually > 20 ppbv, (Wang
 315 et al., 2022; Yang et al., 2022; Yun et al., 2018b) and higher than those on the remote islands

316 in South China Sea (< 5 ppbv, Chuang et al., 2013). The mixing ratio of NO at nighttime
 317 was low and showed small peaks during daytime. With the O₃ accumulating throughout
 318 the day, NO decreased to below the instrument detection limit in the first half of the night,
 319 while it began to increase as the O₃ concentration decreased in the second half of the night.
 320 Given that the lifetime of NO is only a few minutes in the presence of several tens of ppbv
 321 of O₃ (Dewald et al., 2022), we inferred that NO is likely ~~to come~~originated from a local
 322 source such as soil emission, boats, cooking, and so on.

323 **Table 2.** Summary of ~~detailed information~~parameters on the two air mass types (mean ±
 324 standard deviation).

Species	IAM		CAM	
	All day ^b	Nighttime ^b	All day	Nighttime
O ₃ (ppbv)	45.8 ± 20.2	42.9 ± 18.4	53.1 ± 11.9	51.4 ± 9.6
NO _x (ppbv)	15.1 ± 8.7	14.5 ± 9	9.2 ± 5.1	8.8 ± 4.8
NO ₂ (ppbv)	13.9 ± 7.6	14.1 ± 8.3	8.6 ± 4.8	8.6 ± 4.8
NO (ppbv)	1.2 ± 2.3	0.4 ± 1.1	0.5 ± 0.6	0.2 ± 0.1
Temp (°C)	19.9 ± 2	19.9 ± 1.9	20.8 ± 1.5	20.6 ± 1.5
RH (%)	46.7 ± 12.5	47.7 ± 13.2	61.2 ± 10	64.1 ± 9.6
P(NO ₃) (ppbv h ⁻¹)	1.6 ± 0.9	1.5 ± 0.8	1.3 ± 0.8	1.2 ± 0.6
N ₂ O ₅ (pptv)	- ^c	119.5 ± 128.6	- ^c	-
NO ₃ (pptv) ^a	-	9.9 ± 12.5	-	-
τ _{N₂O₅} (min)	-	6.5 ± 6.5	-	-
τ _{NO₃} (min)	-	0.5 ± 0.7	-	-

325 Note: ^a NO₃ is calculated by the thermal equilibrium between NO₂, NO₃, and N₂O₅.

326 ^b “All day” means the 24-hour average and the “Nighttime” means the time between 18:00-
 327 06:00 local time.

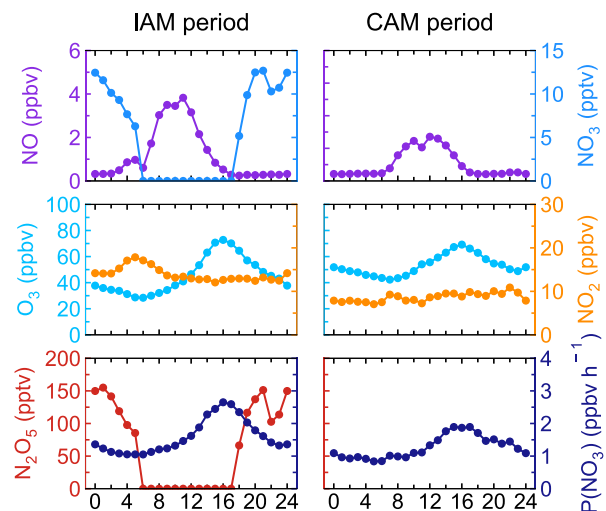
328 ^c Without N₂O₅ measurement in the daytime and limited N₂O₅ data during the CAM period,
 329 N₂O₅, NO₃, and their lifetimes were not valid here.

330 N₂O₅ was at a moderate level on most days with a nocturnal average of 119.5 ± 128.6 pptv,
 331 with high concentrations (>400 pptv in 1-hour average) only lasting for in the first three
 332 days during this campaign. During the nights from November 9th to 12th, the N₂O₅
 333 concentrations were significantly higher than those at on other nights, with a maximum of
 334 657.3 pptv at midnight of November 12th. The NO₃ concentration (calculated based on the
 335 thermal equilibrium with N₂O₅) was also moderate with an average mixing ratio of 9.9 ±
 336 12.5 pptv, which was higher than that reported on a nearby coastal site of Hong Kong Island
 337 (Yan et al., 2019). Table 3 compares the N₂O₅, NO₃, and P(NO₃) found in other coastal (or
 338 island) and continental regions from Europe, the United States, and China. In our study,

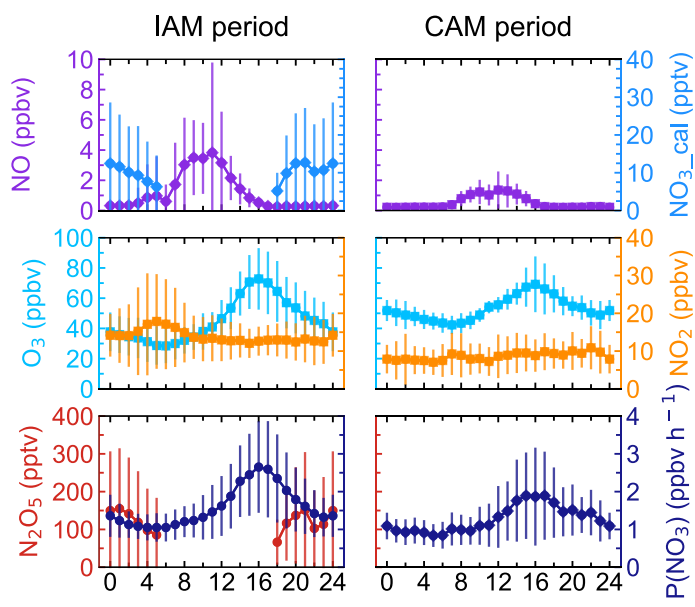
339 N₂O₅ and NO₃ were at a moderate level compared to other coastal regions when they were
340 affected by emission plumes from continental regions, such as Northwestern Europe
341 (Morgan et al., 2015), the East coast of the USA (Brown et al., 2004), and Shenzhen, China
342 (Niu et al., 2022), and were comparable with urban regions (Wang et al., 2017b; Wang et
343 al., 2018b). The concentrations of NO₃ precursors (NO₂ and O₃) at this site were much
344 similar to some rural areas, leading to a high NO₃ production rate with a daily average of
345 1.5 ± 0.9 ppbv h⁻¹ and a maximum of 5.9 ppbv h⁻¹. The average value is much higher than
346 that reported in Beijing in winter (0.4 ppbv h⁻¹, (Wang et al., 2021), comparable to autumn
347 (1.4 ± 1.7 ppbv h⁻¹, (Wang et al., 2017b) and even higher than that in summer Taizhou (1.01
348 ± 0.47 ppbv h⁻¹, (Wang et al., 2020a). The nocturnal average P(NO₃) during this campaign
349 was 1.4 ± 0.7 ppbv h⁻¹, even which is higher than the average value in the warm season of
350 China with 1.07 ± 0.38 ppbv h⁻¹ (Wang et al., 2023). Besides the high NO₂ and O₃, the
351 high reaction rate constant for NO₂ and O₃ due to the high temperature at this site is a
352 potential explanation for the high P(NO₃) values observed in this study: (i.e., at same NO₂
353 and O₃ level, if temperature increased from 10 °C to 20 °C, the reaction rate constant would
354 increase from 2.27×10^{-17} to 3.05×10^{-17} , which means the P(NO₃) would be 1.34 times
355 faster). The high P(NO₃) and the low concentrations of N₂O₅ and NO₃ indicate intensive
356 atmospheric oxidation capacity and fast NO₃ and N₂O₅ removal over the Pearl River
357 Estuary.

358 ~~The difference of trace gases in IAM and CAM periods, and the~~The mean diurnal profiles
359 of N₂O₅, together with relevant species are shown in Fig. 3. Daytime N₂O₅ and NO₃ in the
360 IAM period were shown as ~~zero~~NaN due to the absence of observation. Because of limited
361 N₂O₅ data for the CAM period, neither N₂O₅ nor NO₃ is shown in Fig. 3. NO exhibited
362 similar diurnal variation in both periods and the mixing ratio was higher in the IAM period.
363 The wind rose plot (Fig. S1) showed high concentrations of NO originating from the north
364 characterized by the outflow from PRD regions. However, NO₂ differed in the two periods,
365 showing highly high anti-correlation with O₃ only in the IAM period and little diurnal
366 variation in the CAM period. ~~A fit of nocturnal O₃ against NO₂ (Fig. S2) yields a slope of~~
367 ~~-1.1 in IAM, implying that the major emission of NO_x was NO and almost no nocturnal~~
368 ~~NO₂ production occurred (Brown et al., 2016).~~

369



370



371 **Figure 3.** Mean diurnal profiles of N_2O_5 , NO_3 , $P(NO_3)$, and relevant parameters in the two
 372 types of air masses. NO_3 was calculated from N_2O_5 . Neither N_2O_5 nor NO_3 was shown
 373 during CAM period because of limited N_2O_5 measurement.

374 Ozone exhibited a typical diurnal pattern for all air masses, gradually increasing
 375 until its peak at 16:00 and then slowly decreasing throughout the night until its lowest
 376 mixing ratio was reached at about 06:00. Compared to the CAM period, the lower
 377 minimum hourly O_3 concentration and a small peak of NO_2 in the early morning indicated
 378 that NO titration effect was stronger in the IAM period, and the higher maximum of O_3
 379 concentration in IAM indicated that photochemical formation of O_3 and/or transport was
 380 faster to completely offset the titration. In addition, the higher NO_x and VOC

381 concentrations (as shown in Table S1) in the IAM period facilitated O₃ formation. With the
382 elevated precursor concentrations (NO₂ and O₃) in the IAM period, N₂O₅ and NO₃
383 accumulated rapidly after sunset, reaching their peak values (~~155.04~~92.1 pptv and 49.6
384 pptv for each) ~~near 20:00.~~ P(NO₃) was highly consistent with O₃ in diurnal variation and
385 reached the peak at 16:00, with peak values of 2.7 ppbv h⁻¹ (IAM) and 1.9 ppbv h⁻¹ (CAM),
386 as well as a nocturnal average value of 1.5 ± 0.8 ppbv h⁻¹ (IAM) and 1.2 ± 0.6 ppbv h⁻¹
387 (CAM), respectively. The P(NO₃) of CAM was consistent with the observation ~~in~~when the
388 air mass over eastern Shenzhen was transported from the clean area or sea surface (1.2 ±
389 0.3 ppbv h⁻¹), (Niu et al., 2022) ~~during which the air masses were transported from clean~~
390 ~~areas or the sea surface.~~

391 .

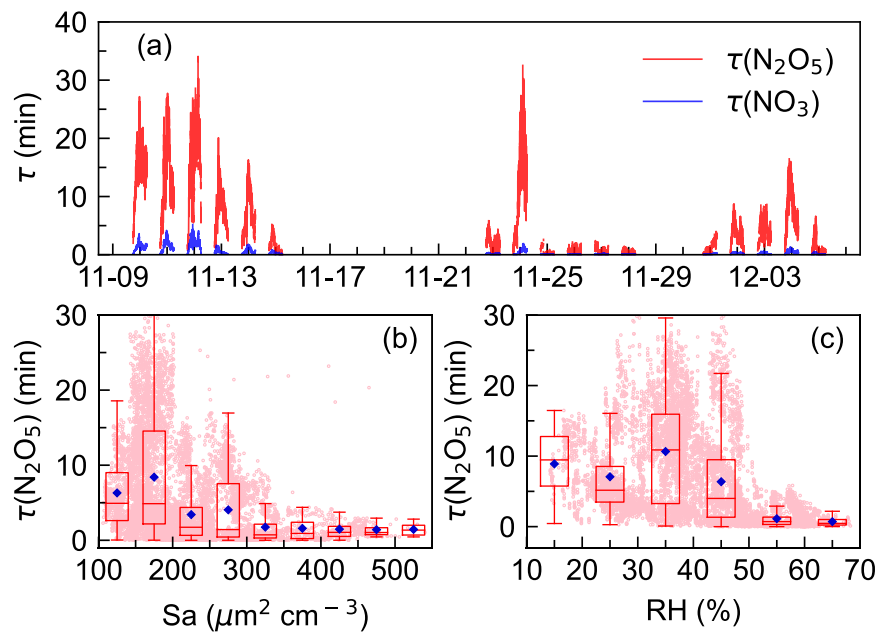
392 **Table 3.** Summary of field-observed N₂O₅, NO₂, O₃ concentrations, and NO₃ production rate.

Region	Location	Time	N ₂ O ₅ (pptv)	NO ₃ (pptv)	NO ₂ (ppbv)	O ₃ (ppbv)	<i>P</i> (NO ₃) (ppbv hr ⁻¹)	References
Urban	Jinan, China	Aug.-Sep., 2014	22 ± 13 (max 278)		74.6	55	/	(Wang et al., 2017c)
Urban	Shanghai, China	Aug.-Oct., 2011	310 ± 380	16±9 (max 95)	0-76	23 ± 8 (max 57)	1.10 ± 1.09	(Wang et al., 2013)
Urban	Beijing, China	May-Jul., 2016	100–500 (max 937)	27	/	/	1.2 ± 0.9	(Wang et al., 2018b)
Urban	Mt. Tai, China	Jul.-Aug., 2014	6.8±7.7	/	16.4 (±6.1)	88.6 (±16.6)	0.45±0.40	(Wang et al., 2017d)
Urban	Heshan, China	Sep.-Nov., 2019	64 ± 145 (night) (max 1180)	max 90	21.0±10.4	75.2±20.9 (max 152.8)	2.5 ± 2.1 (day) 1.8 ± 1.5 (night)	(Wang et al., 2022)
Urban	Beijing, China	Sep.-Oct., 2019	68.0 ± 136.7	/	35.1 ± 16.6	27.7 ± 25.2	2.25 ± 2.02	(Wang et al., 2017b)
Suburban	Changzhou, China	May-Jul., 2019	53.4 ± 66.1 (max 304.7)	4.7 ± 3.5 (max 17.7)	13.7 ± 8.9	48.4 ± 27.8	1.7 ± 1.2 (max 7.7)	(Lin et al., 2022)
Rural	Wangdu, China	Jun.-Jul., 2014	<200 (max 430)	/	10-80	(max 146)	1.7 ± 0.6	(Tham et al., 2016)
Rural	Taizhou, China	May-Jul., 2018	26.0 ± 35.7 (max 492)	4.4 ± 2.2 (max 150)	28.28 ± 18.57	48.2 ± 32.5	1.01 ± 0.47 (night)	(Wang et al., 2020a)
Coastal	Tai Mo Shan, HK	Nov.-Dec., 2013	0.5-11.8 ppbv	-	7.88	68.5	0.01-2	(Brown et al., 2016)
Coastal	East coast of USA	Jun.-Aug., 2002	85	17	6	35	/	(Brown et al., 2004)
Coastal	California, USA	Jan., 2004	0-200	/	0-15	15–35	/	(Wood et al., 2005)
Coastal	Southern Spanish	Nov.-Dec., 2018	~500 (max)	/	1-15	15-40	/	(Crowley et al., 2011)
Coastal	Shenzhen, China	Sep.-Oct., 2019	55.6 ± 89 (max 1420) 45.4 ± 55.2 (BAM)	/	6.2	88.9±24.6	2.9 ± 0.5 (UAM) 1.2 ± 0.3 (BAM)	(Niu et al., 2022)
Coastal	Northwestern Europe	Jul., 2010	670	/	0.5–2	30– 40	/	(Morgan et al., 2015)
Island	Hok Tsui, HK	Aug.-Sep., 2012	17±33 (max 336)	7 ± 12	6 ± 7	33 ± 24	/	(Yan et al., 2019)
Island	Wanshan, China	Nov.-Dec., 2021	107.22 ± 125.17	7.56 ± 10.95	13.14 ± 8.68	43.75 ± 18.49	1.38 ± 0.83	This work

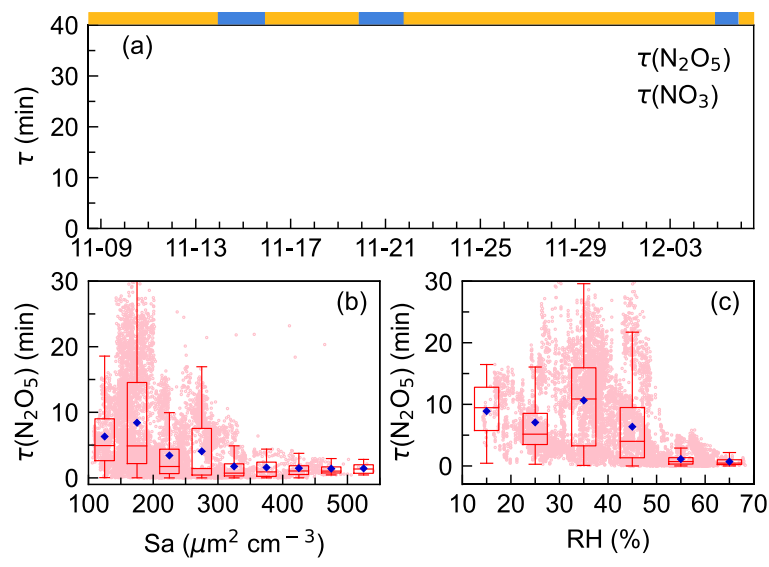
393 Notes: UAM means air masses coming from continental areas, and BAM means air masses coming from background marine areas.
 394 Mean values are in the form of mean ± standard deviation or single data. The maximum was noted in the table.

395 **3.2 The lifetimes of N₂O₅ and NO₃**

396 Steady-state lifetime is one of the most common and useful diagnostics for NO₃ and N₂O₅
397 analysis in the atmosphere (Brown et al., 2003; Wang et al., 2018b; Wang et al., 2020a;
398 Brown et al., 2016). As shown in Fig. 4, τ_{NO_3} was low during the whole campaign with
399 an average of 0.5 ± 0.7 min. $\tau_{N_2O_5}$ showed a similar pattern to τ_{NO_3} but had a much
400 higher value, ranging from 0 to 34.1 min with an average of 6.1 ± 6.5 min. The N₂O₅
401 lifetime was higher in the first half of the campaign (11.5 min, November 9th to 14th) than
402 in the second half (3.5 min, November 22th to 28th). The difference was mainly due to the
403 N₂O₅ mixing ratio rather than P(NO₃), as P(NO₃) shows no significant difference during
404 the whole observation (Fig. 2).



405



406

407 **Figure 4.** Time series of N_2O_5 and NO_3 lifetimes (a) and variations of nocturnal N_2O_5
 408 lifetime as a function of aerosol surface area density, S_a (b), and relative humidity, RH (c).
 409 The blue diamond represents the average $\tau_{\text{N}_2\text{O}_5}$ and pink dots represent the scatter data
 410 point in 1 min. The ribbon at the top separates the air masses into two categories, yellow
 411 for IAM and blue for CAM.

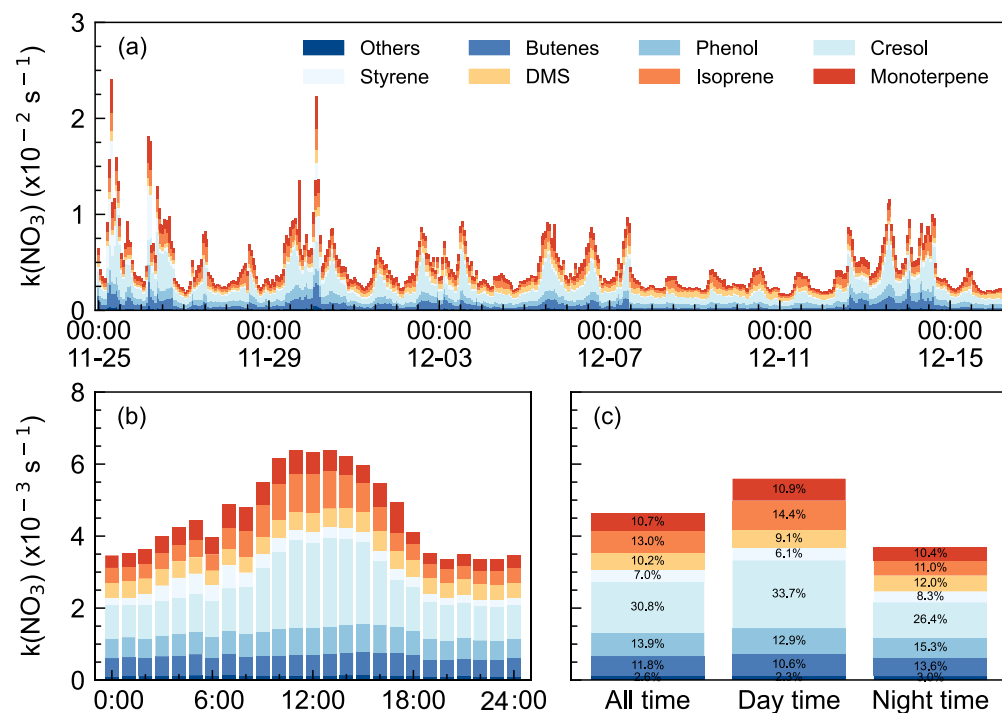
412 $\tau_{\text{N}_2\text{O}_5}$ values were comparable to those measured on the coastline of Finokalia, Greece for
 413 a median of 5 min (Vrekoussis et al., 2004; Vrekoussis et al., 2007), but much lower than
 414 those previously reported in the residual layer in Hong Kong for 1-5 h (Brown et al., 2016).
 415 In comparison, the lifetimes were much longer than in inland urban areas, for example,
 416 0.93 ± 1.13 min in Taizhou (Li et al., 2020), 1.6 ± 1.5 min in Changzhou (Lin et al., 2022)
 417 for YRD regions, 1.1-10.7 min (Zhou et al., 2018) and 4.5 ± 4.0 min (Wang et al., 2018b)
 418 in Beijing. Typically, high aerosol loading, more intensive VOC, and NO emissions in these
 419 areas led to enhanced N_2O_5 uptake and reactions of NO_3 with VOC. But at this site, the
 420 atmosphere was relatively clean since the maximum S_a value was less than $600 \mu\text{m}^2 \text{cm}^{-3}$,
 421 making N_2O_5 uptake slow. While in this site, measurement indicated that the peak diameter
 422 in the particle number distribution was small during the whole campaign and indicated no
 423 significant difference between two air masses with respect to the aerosol diameters (Fig.
 424 S2). S_a value ranged from $29 \mu\text{m}^2 \text{cm}^{-3}$ to $557 \mu\text{m}^2 \text{cm}^{-3}$. All of these indicated the
 425 atmosphere was relatively clean (Wang et al., 2017b), making N_2O_5 uptake slow. Fig. 4b
 426 shows N_2O_5 lifetime decreased rapidly from 8.3 min to 1.7 min when S_a increased up to
 427 $300 \mu\text{m}^2 \text{cm}^{-3}$ and then remained at relatively low constant levels though S_a still increased.
 428 Such a trend of $\tau_{\text{N}_2\text{O}_5}$ - S_a dependence was consistent with previous observations and varied
 429 in exact values (Zhou et al., 2018; Wang et al., 2018b; Li et al., 2020). Fig. 4c. showed that

430 $\tau_{\text{N}_2\text{O}_5}$ decreased as RH increased ($> 40\%$) possibly due to the hygroscopic aerosol growth
431 and the dependence of the N_2O_5 uptake coefficient on the RH (Brown and Stutz, 2012).
432 Overall, the trend is consistent with previous works, while the large discrepancy of the
433 dependence implied that N_2O_5 uptake was not the dominant NO_3 loss process.

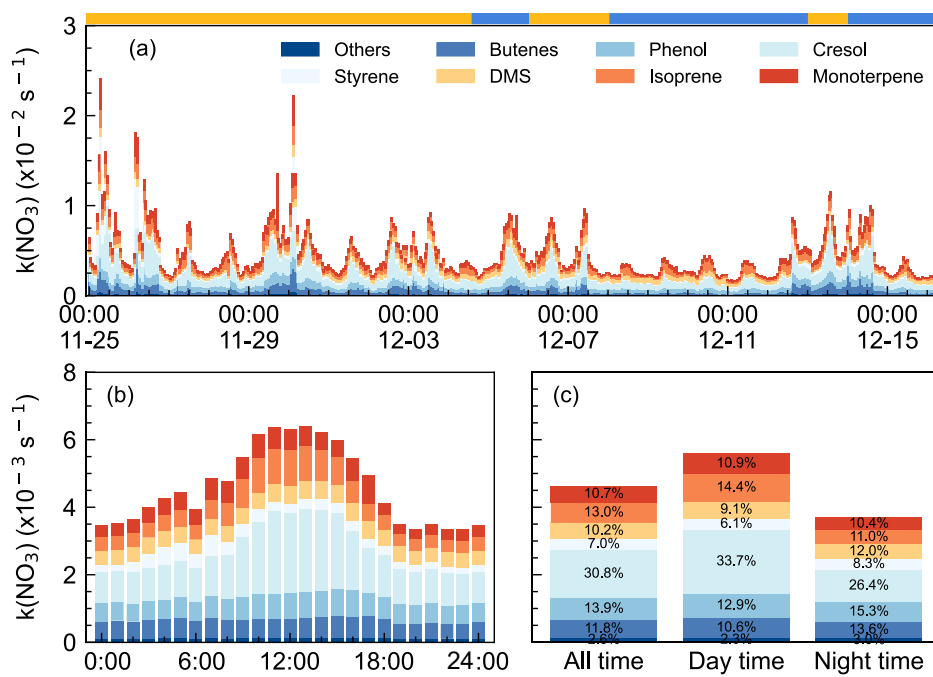
434 3.3 The NO_3 reactivity and N_2O_5 uptake coefficients

435 The concurrent high $P(\text{NO}_3)$ and low NO_3 lifetime imply high NO_3 reactivity as well as a
436 large nocturnal NO_3 loss process at DWS. The NO_3 reactivity ($k(\text{NO}_3)$) towards VOCs was
437 calculated by Eq. 4, towards which were categorized into anthropogenic VOC and biogenic
438 VOC (Gu et al., 2021). Throughout the campaign, $k(\text{NO}_3)$ varied considerably (Fig. 5a),
439 showing relatively high and fluctuated values when the airmasses featured IAM. The
440 $k(\text{NO}_3)$ ranged from $1.6 \times 10^{-3} \text{ s}^{-1}$ to $2.4 \times 10^{-2} \text{ s}^{-1}$ with the daily average of $4.6 \pm 2.8 \times 10^{-3}$
441 s^{-1} . Low values of $k(\text{NO}_3)$ were observed from December 9th to 12th when the air masses
442 originate from coastal or offshore from the east and southeast, which features the outflow
443 of coastal cities like Hong Kong and Shenzhen.

444 Fig. 5b shows the mean diurnal profile of $k(\text{NO}_3)$, where a trend of high values in the
445 daytime and low values at nighttime are observed. Anthropogenic VOC, especially cresol,
446 dominated the daily trend of $k(\text{NO}_3)$, while biogenic VOC- $k(\text{NO}_3)$ showed no significant
447 diurnal variation. Except cresol, other highly reactive VOC showed little change
448 throughout the day. Regarding the biogenic VOC- $k(\text{NO}_3)$, the concentrations of
449 monoterpene, isoprene, and DMS changed smoothly although their emissions would
450 increase with elevated temperature and sunlight during daytime (Fuentes. et al., 2000). The
451 detailed contributions of VOC categories to $k(\text{NO}_3)$ were shown in Fig. 5c. The $k(\text{NO}_3)$
452 was $5.6 \pm 2.8 \times 10^{-3} \text{ s}^{-1}$ and $3.7 \pm 2.5 \times 10^{-3} \text{ s}^{-1}$ on average for daytime and nighttime,
453 respectively. The daytime distribution of $k(\text{NO}_3)$ differed from that at the mountaintop of
454 Tai Mo Shan in Hong Kong (Brown et al., 2016). During the nighttime, anthropogenic
455 VOC- $k(\text{NO}_3)$ tripled the biogenic VOC- $k(\text{NO}_3)$ and was dominated by cresol (26.4%). The
456 nighttime $k(\text{NO}_3)$ corresponded to a NO_3 lifetime of 4.5 min, which was about 10 times the
457 lifetime derived from steady-state analysis, indicating that the reaction of NO_3 with VOC
458 was not significant enough. The faster NO_3 loss rate also indicated the less aged air mass
459 that was influenced by surface-level emissions.



460



461

462 **Figure 5.** NO_3 reactivity via VOCs during the campaign. (a) $k(\text{NO}_3)$ time series from Nov.
 463 25th to Dec. 15th; (b) mean diurnal profiles; and (c) the relative contribution in different
 464 categories. The ribbon at the top separates the air masses into two air masses types, yellow

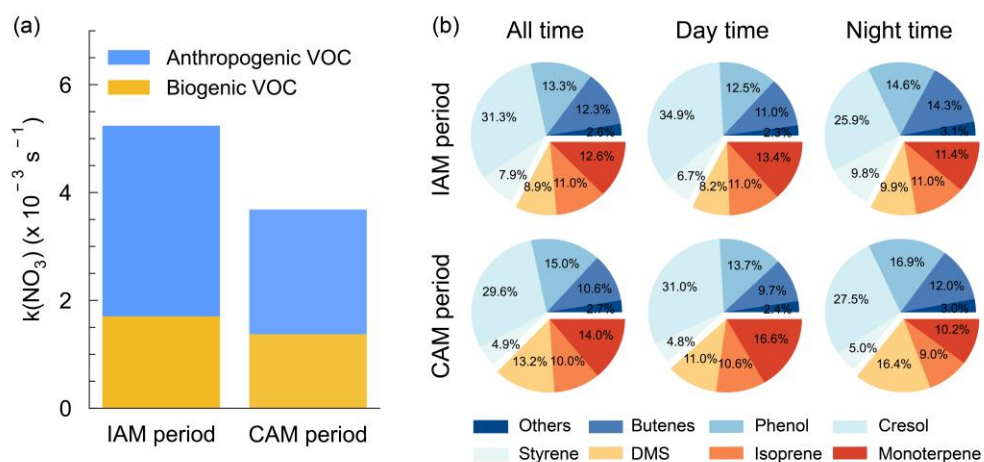
465 for IAM and blue for CAM.

466 We showed that NO₃ reactivity and its composition in this study exhibited significant
467 differences compared to other urban or forested regions (Wang et al., 2017d; Ayres et al.,
468 2015; Brown et al., 2016; Lin et al., 2022). Although anthropogenic VOCs played a
469 dominant role, accounting for 66.1%, the major contributors were not low-carbon alkenes
470 but phenol (13.9%, $0.64 \pm 0.28 \times 10^{-3} \text{ s}^{-1}$) and cresol, (30.8%, $1.4 \pm 1.0 \times 10^{-3} \text{ s}^{-1}$), which
471 have received little attention in previous studies. Despite their relatively low concentrations,
472 averaging 7 ± 3 pptv and 4 ± 3 pptv respectively, their substantial contribution to $k(\text{NO}_3)$
473 is notable due to their fast rate constants ($3.8 \times 10^{-12} \text{ cm}^3 \text{ molecule}^{-1} \text{ s}^{-2}$ and $1.4 \times 10^{-11} \text{ cm}^3$
474 $\text{molecule}^{-1} \text{ s}^{-2}$ at 298 K, respectively) for reaction with NO₃. ~~These substances are mainly~~
475 ~~secondary species from aromatic compounds and significantly higher concentrations have~~
476 ~~also been observed in urban areas (Delhomme et al., 2010; Zhu et al., 2005; Belloli et al.,~~
477 ~~1999).~~ Considering that the measured phenol and cresol concentration is low and near the
478 instrumental detection limit, we note this may bring some uncertainties in quantifying the
479 contribution to the total NO₃ reactivity and NO₃ loss rate. These substances are mainly
480 secondary species from aromatic compounds and higher concentrations have also been
481 observed, such as in the Strasbourg area, France (14 pptv, Delhomme et al., 2010) and in
482 Great Dun Fell, UK (16 pptv, Lüttke et al., 1997). Hence, these phenolic compounds were
483 potentially important but often overlooked for their contributions to NO₃ reactivity in urban
484 areas, and their reactions with NO₃ may also contribute to the formation of nitrophenol.
485 These reactions warrant further attention in future research. Regarding biogenic VOCs,
486 besides the contributors commonly observed in forest regions such as monoterpenes and
487 isoprene, the marine emissions indicator, dimethyl sulfide (DMS), contributed 10.2% to
488 NO₃ reactivity (daily average). Previous studies have suggested that DMS may serve as a
489 major direct sink for NO₃ in clean marine regions (Allan et al., 1999; Aldener et al., 2006;
490 Brown et al., 2007). However, this study reveals that anthropogenic VOC emissions
491 significantly enhanced the NO₃ reactivity in marine areas, highlighting the crucial influence
492 of anthropogenic activities on marine atmospheric chemistry.

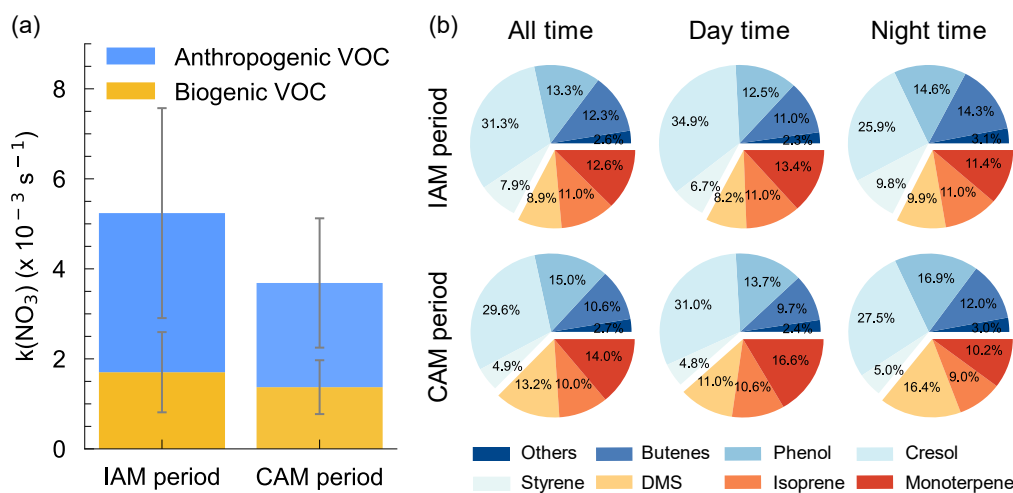
493 As shown in Fig. 6a, $k(\text{NO}_3)$ differed significantly between the inland and coastal air
494 masses, with $5.2 \pm 3.1 \times 10^{-3} \text{ s}^{-1}$ and $3.7 \pm 1.9 \times 10^{-3} \text{ s}^{-1}$ on average in IAM and CAM periods,
495 respectively. Of which anthropogenic VOC- $k(\text{NO}_3)$ in IAM ($3.5 \pm 2.3 \times 10^{-3} \text{ s}^{-1}$) was higher
496 than in CAM ($2.3 \pm 1.4 \times 10^{-3} \text{ s}^{-1}$) and dominant in both air masses, while biogenic VOC-
497 $k(\text{NO}_3)$ was comparable. ($1.7 \pm 0.9 \times 10^{-3} \text{ s}^{-1}$ and $1.4 \pm 0.6 \times 10^{-3} \text{ s}^{-1}$ for IAM and CAM,
498 respectively). The difference indicated that this region was affected by long-range transport
499 emissions to a certain extent. The pie charts in Fig. 6b showed different VOC categories
500 that contributed to $k(\text{NO}_3)$ in two periods with AVOC dominant at any time. The change in
501 the relative contribution of various VOCs to $k(\text{NO}_3)$ varied simultaneously throughout the

502 day, ~~reflecting as~~ showing an increase in butene, phenol, and DMS ~~increased, while, and a~~
 503 decrease in cresol and monoterpene ~~decreased~~ from daytime to nighttime.

504 N₂O₅ heterogeneous uptake on aerosol is one of the vital loss processes of NO₃ and the
 505 uptake coefficient varied greatly under different environmental conditions. For instance,
 506 $\gamma(\text{N}_2\text{O}_5)$ can reach up to 0.072 in polluted urban regions (Wang et al., 2017b; Wang et al.,
 507 2018b; Lu et al., 2022; Li et al., 2020), while usually below 0.03 in coastal areas (Brown
 508 et al., 2016; Morgan et al., 2015; Niu et al., 2022). N₂O₅ uptake coefficient can be gotten
 509 from the pseudo steady state method by assuming that N₂O₅ and NO₃ have achieved a
 510 steady state (Brown et al., 2009), in which the fitted slope represents $\gamma(\text{N}_2\text{O}_5)$ and the
 511 intercept represents the direct loss rate coefficient, $k(\text{NO}_3)$ ~~(as shown in Eq. 8)~~. However,
 512 this approach failed to generate valid results in our study since a negative slope or intercept
 513 was observed (Fig. ~~S3S4~~). These results indicated that a large NO₃ removal process existed
 514 at this site, making it unable to approach a stable state. ~~Based on relative humidity and~~
 515 ~~temperature, we~~ The $\gamma(\text{N}_2\text{O}_5)$ was also calculated the uptake coefficient by Eq. 6
 516 from November Nov. 9th to 16th by using the simplified parameterization, as shown in Eq. 9. The
 517 parameterized average $\gamma(\text{N}_2\text{O}_5)$ showed a large variation ranging from 0.0014 to 0.0299,
 518 with an average of 0.0095 ± 0.0059 . This value is within the range from <0.0016 to 0.03
 519 derived from the ambient observation around other coastal areas (Niu et al., 2022; Yun et
 520 al., 2018a; Brown et al., 2006; Brown et al., 2016; Morgan et al., 2015) and smaller than
 521 the polluted North China Plain (Wang et al., 2017c; Wang et al., 2017b; Wang et al., 2017d;
 522 Tham et al., 2018).



523



524

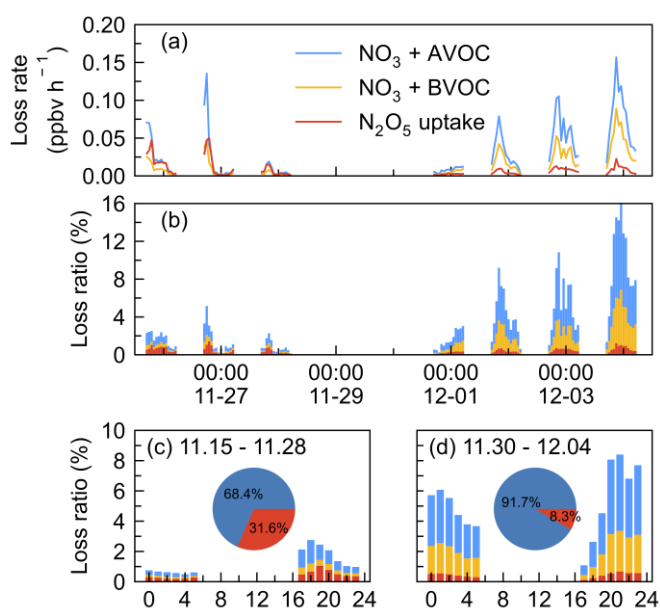
525 **Figure 6.** (a) Distributions of $k(\text{NO}_3)$ in continental from AVOC and coastal air
 526 masses. BVOC for both IAM and CAM period. The error bar indicates the standard
 527 deviation. (b) The relative contribution of VOC categories to the $k(\text{NO}_3)$.

528 3.4 The NO_3 loss budget

529 To assess the contribution of various loss processes to the total NO_3 removal, we calculated
 530 their loss rate and the loss ratio, $LR(\text{NO}_3)$. Considering the $LR(\text{NO}_3)$ is defined as the short
 531 lifetimesum of NO_3 the loss rate by process X (VOC or N_2O_5 uptake) to the total NO_3 loss
 532 rate, here the total NO_3 loss rate is represented by $P(\text{NO}_3)$ which characterizes the
 533 atmospheric oxidation capacity since we cannot quantify the total NO_3 loss rate due to the
 534 NO concentration below the limit of NO_3 to its reactants instrument detection. Due to the
 535 data absence of measured VOCs or N_2O_5 during certain periods, the loss proportion of
 536 VOCs and N_2O_5 uptake in NO_3 loss only presented from Nov. 26th to Dec. 5th during which
 537 all air masses originated from continental China. As shown in Fig. 7, a closer examination
 538 revealed that the nights can be divided into two periods, period I: November 25th to 28th
 539 when the loss ratio of VOC and N_2O_5 uptake remained below 3%, and period II: November
 540 30 to December 4 when the loss ratio was higher. Both periods had large nocturnal NO_3
 541 production rates with an average of 2.1 ± 1.1 ppbv h^{-1} in period I and 1.4 ± 0.6 ppbv h^{-1}
 542 in period II, respectively.

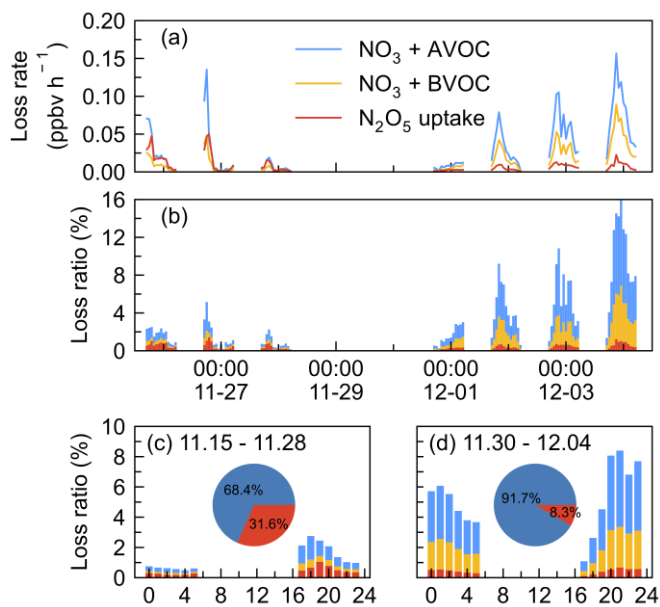
543 N_2O_5 uptake rate was larger in period I (0.01 ± 0.01 ppbv h^{-1}) than that in period II (0.006
 544 ± 0.004 ppbv h^{-1}), which can be explained by the increased RH, Sa, and N_2O_5 concentration
 545 as shown in Fig. 2. The loss ratio of these processes was shown in Fig. 7b, the total NO_3
 546 loss through reactions with VOCs and N_2O_5 uptake accounted for less than 20%, with an

547 average of 1.2% (period I) and 5.3% (period II), respectively. This result shows that the
 548 nighttime NO_3 chemistry may be almost negligible, to the NO_x removal compared with
 549 the NO_x removal capacity during the day $\text{OH} + \text{NO}_2$ pathway according to previous works
 550 reported in urban regions (Wang et al., 2017b; Wang et al., 2020a). The diurnal variation
 551 of the NO_3 loss fraction of both periods was shown in Fig. 7c and 7d, revealing that NO_3
 552 loss via N_2O_5 uptake and VOCs was slightly higher in the early evening and relatively
 553 stable in the late evening. The pie charts in the center were the relative contribution between
 554 VOCs and N_2O_5 uptake, showing that VOCs were overwhelming compared with N_2O_5
 555 uptake during the two periods, with an average of 68.4% and 91.7% during the first and
 556 second periods, respectively.



557

558 To better understand the nocturnal oxidation of VOCs, we compared the nighttime
 559 oxidation of VOCs by NO_3 with O_3 . Since OH was not measured and OH is often regarded
 560 as a vital daytime oxidant (Finlayson-Pitts, 2000; Lu et al., 2010), we did not consider OH
 561 oxidation in the nighttime. Figure S4 showed the diurnal pattern of VOC loss rate by NO_3
 562 and O_3 , NO_3 predominantly achieves its peak oxidation rates (0.07 ppbv h^{-1}) during the
 563 initial half of the night, accounting for 63.1% of the total VOC oxidation on nocturnal
 564 average. Meanwhile, O_3 also makes a contribution to VOC oxidation, mainly owing to its
 565 relatively high nighttime concentration levels (42.9 ± 18.4 ppbv).

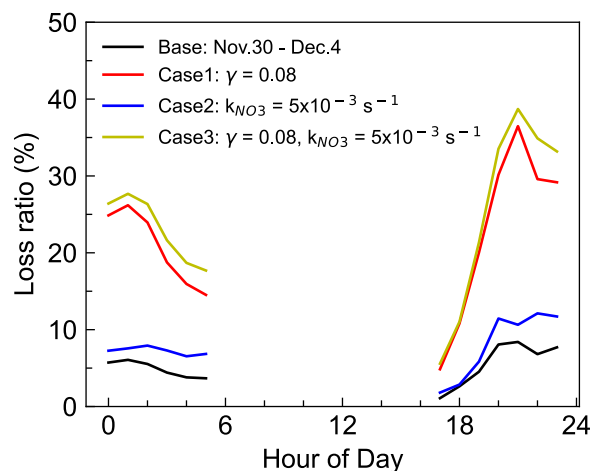


566

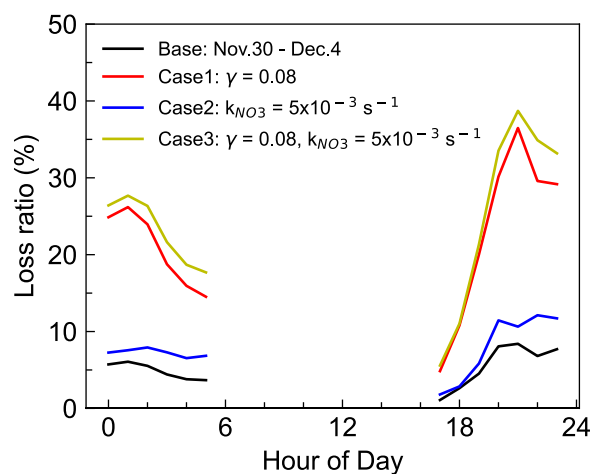
567 **Figure 7.** Time series of (a) the loss rate of NO_3 reactions with AVOC, BVOC, and N_2O_5 uptake, and (b) fractional contribution to the NO_3 loss during the nighttime by taking
 568 $P(\text{NO}_3)$ as the total NO_3 loss in the IAM period. The mean diurnal profiles of NO_3 loss
 569 ratio in two periods (c) November 25th - 28th, and (d) November 30th - December 4th. Pie
 570 charts in the center showed the relative contribution of VOCs (blue) and N_2O_5 uptake (red)
 571 in NO_3 loss.
 572

573 Due to the difficulty in experimental quantifying $\gamma(\text{N}_2\text{O}_5)$, the estimation of N_2O_5 uptake
 574 in NO_3 loss may include some uncertainty. Considering the uncertainty both in
 575 parameterized $\gamma(\text{N}_2\text{O}_5)$ and the NO_3 reactivity calculation, three sensitivity tests were
 576 conducted to assess the uncertainty in period II because of the relatively high loss ratio in
 577 the above analysis (Fig. 8), and the three cases were used to represent the upper limit of
 578 their contribution to NO_3 loss. Case 1 represents the overrated contribution of N_2O_5 uptake
 579 by taking $\gamma(\text{N}_2\text{O}_5) = 0.08$, which was the high value reported in high N_2O_5 and ClNO_2
 580 plume of Shenzhen (Niu et al., 2022) and approximately seven times the parameterized
 581 value at this site. In this case, the fraction of $\text{NO}_3 + \text{VOCs}$ and N_2O_5 uptake was significantly
 582 elevated to account for approximately 30% of NO_3 loss. Case 2 shows the total NO_3
 583 reactivity reached an average of $5.0 \times 10^{-3} \text{ s}^{-1}$ by taking β -pinene as the total monoterpene
 584 because of the higher reaction rate constant. The weak change in the loss ratio indicates the
 585 reactions of NO_3 with VOC may not be sensitive to the weights of monoterpenes, since the
 586 contribution of monoterpenes to the NO_3 reactivity is not dominant. Case 3 is the synthesis
 587 of Case 1 and Case 2 by considering higher N_2O_5 uptake coefficient and higher $k(\text{NO}_3)$ to
 588 represent the upper limit of N_2O_5 uptake and NO_3 reaction with VOCs to NO_3 loss, whose

589 result is slightly higher than the contribution of Case 1. Nevertheless, the quantified upper
590 contribution was still less than half. Thus, we conclude that most of the NO_3 loss was not
591 well accounted for even considering the uncertainties.



592



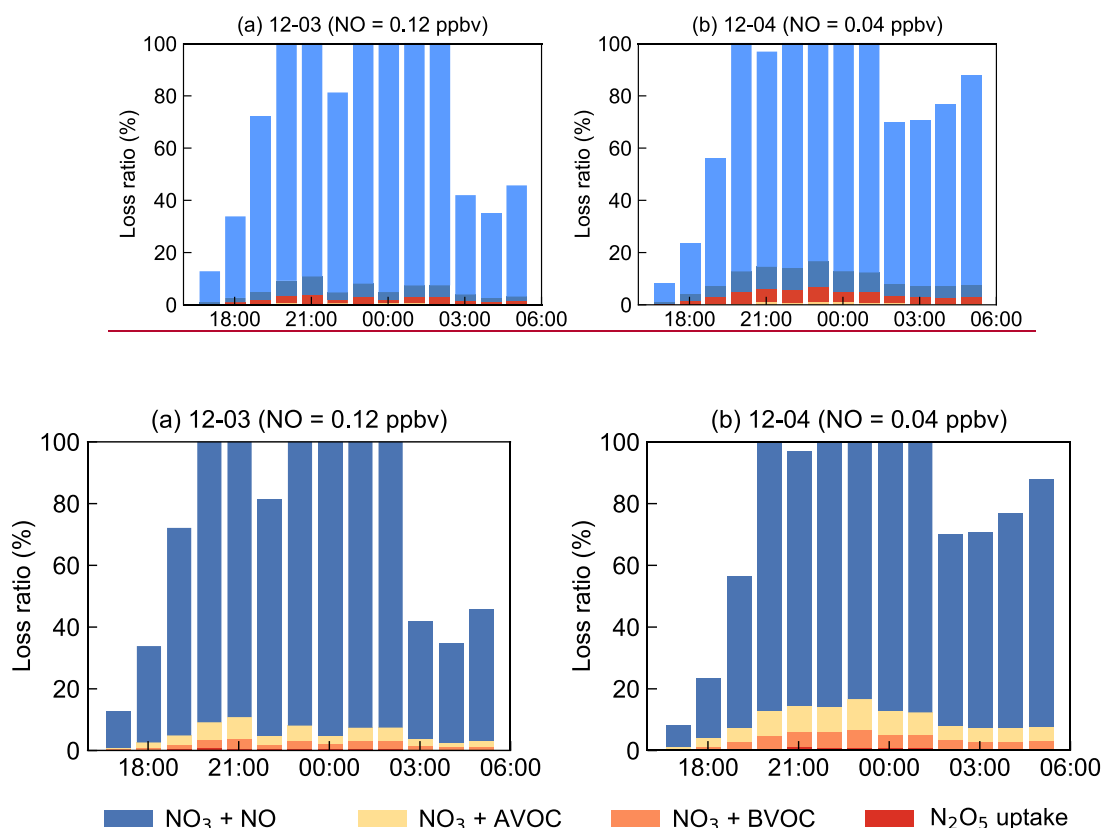
593

594 **Figure 8.** Three sensitivity tests for the contribution of VOCs and N_2O_5 uptake to the NO_3
595 loss during the nighttime of period II (November 30th - December 4th). Case 1 takes $\gamma(\text{N}_2\text{O}_5)$
596 = 0.08, which is the high value reported in the previous study. Case 2 takes β -pinene as the
597 total monoterpene with a higher reaction rate constant, and Case 3 is the synthesis of the
598 above two cases to represent the upper limit of the contribution.

599 The NO_3 reaction with NO was often considered to be one of the dominant loss processes
600 during the daytime since at nighttime NO decreased to low levels, thus not considered in
601 the above analysis. However, by taking NO into consideration although at low
602 concentration levels below the detection limit of the instrument (0.4 ppbv), the contribution

603 of NO to the nighttime NO₃ loss exceeded 100% frequently as shown in Fig. S4S5. Due to
 604 the rapid reaction between NO and NO₃, several pptv concentrations of NO could
 605 effectively account for most NO₃ loss in a relatively clean coastal environment (Crowley
 606 et al., 2011). Nevertheless, limited by NO precise measurement, we considered the
 607 following assessments to understand the total NO₃ loss processes (Fig. 9). By assuming
 608 NO at a constant value of 40-400 pptv, more than 80% of the total NO₃ loss can be well
 609 explained. Although some loss remained unidentified, these results underline that NO,
 610 often considered to be important during daytime, was the predominant NO₃ loss way during
 611 nighttime at this study site. This also suggests accurate measurement of low NO
 612 concentrations is crucial for identifying removal pathways of nocturnal NO₃ oxidants and
 613 has significant implications for nighttime atmospheric chemistry. We can infer that the
 614 nocturnal chemical NO₃ reactions would be largely enhanced once without NO emission
 615 in the open ocean after the air mass passes through this site, indicating the strong influences
 616 of the urban outflow to the downwarddownwind marine areas with respect to nighttime
 617 chemistry.

618



619

620 **Figure 9. Assessments** Examples for the assessment of NO₃ loss process by assuming NO
 621 as constant values. Blue represents the contribution of NO and others are N₂O₅ uptake and

622 VOCs to approximately explain about 80% of the budget.

623 For the absence of measured N_2O_5 during the CAM period, we compared the $k(\text{NO}_3)$ and
624 the reactivity of N_2O_5 uptake ($k_{\text{het}}K_{\text{eq}}\text{NO}_2$) to indirectly reflect NO_3 removal process.
625 Overall, the NO_3 reactivity values from VOCs and N_2O_5 uptake during nighttime was
626 relatively comparable, for 56.5% and 43.5%, respectively. This indicates that VOCs still
627 had a slightly larger contribution than N_2O_5 uptake during the CAM period, which is
628 consistent with the findings in southern China (Brown et al., 2016) and on the east coast of
629 the USA (Aldener et al., 2006).

630 4. Summary and Conclusion

631 This study presents the first observation of nocturnal nitrogen oxide species, N_2O_5 , at a
632 typical marine site (Da Wan Shan Island, Zhuhai) in the north of the South China Sea during
633 the winter of 2021. Although Da Wan Shan Island was almost free of local anthropogenic
634 emissions, the air pollutants from the megacities of the Pearl River Delta were transported
635 to this area by northerly or northeasterly winds during the measurement period. The
636 maximum ratio of N_2O_5 was 657.27 pptv (1 min average) and the nocturnal average was
637 119.5 ± 128.6 pptv. The NO_3 production rate was comparable to that in urban areas such as
638 north China and the Yangtze River Delta, with an average value of 1.5 ± 0.9 ppbv h^{-1} and
639 a maximum of up to 5.84 ppbv h^{-1} , indicating an active nighttime chemical process in that
640 area.

641 Further analysis of N_2O_5 and NO_3 steady state lifetimes indicates that NO_3 had a very short
642 average life of 0.5 ± 0.6 minutes, which was to some extent comparable to that in urban
643 areas in summer. The combination of the high NO_3 production rate and short lifetime
644 suggests a rapid NO_3 loss at night. While N_2O_5 uptake is inefficient in relatively clean air
645 masses. The nighttime $k(\text{NO}_3)$ corresponded to a NO_3 lifetime of 4.5 minutes, indicating
646 that VOCs also contribute little to NO_3 loss. Both VOC and N_2O_5 uptake can only explain
647 less than 20% of the total loss. The fast NO_3 loss rate also indicated the less-aged air mass
648 that was influenced by local surface-level emissions. We infer that the local weak NO
649 emission may significantly change the near-surface chemical pattern of NO_3 chemistry,
650 which may result in a huge difference between the observed results on the island and those
651 on the sea surface. We suggested that future field measurements should be made on sea
652 surfaces away from islands, such as ship-based cruise observation, to get a comprehensive
653 understanding of the nocturnal NO_3 chemistry in the background marine regions.

654

655 **Code/Data availability.** The datasets used in this study are available at:
656 <https://doi.org/10.5281/zenodo.8089100> (Wang et al., 2023).

657 **Author contributions.** H.C.W. and Y. J.T. designed the study. J.W. and H.C.W. analyzed
658 the data with input from H.J.H., Z.L.Z., G.Z.F., C.Z.S., Z.H.L., J.Z., S.J.F.. H.C.W., L.M.
659 Y. J.T., Z.H.L., and J.Z. organized this field campaign and provided the field measurement
660 dataset. J.W., H.C.W., and Y.J.T. wrote the paper. All authors commented on and edited the
661 manuscript.

662 **Acknowledgments**

663 This work was supported by the National Natural Science Foundation of China (Nos.
664 42175111), the Guangdong Major Project of Basic and Applied Basic Research (No.
665 2020B0301030004), Guangdong Basic and Applied Basic Research Foundation
666 (2022A1515010852), and the Fundamental Research Funds for the Central Universities,
667 Sun Yat-sen University (23lgbj002, 23hytd002). L.M. acknowledges the Zhuhai Science
668 and Technology Plan Project (ZH22036201210115PWC).

669
670 **Competing interests.** The authors declare that they have no conflicts of interest.

672 **Appendix A Supplementary data**

673 Supplementary data associated with this article can be found in the online version at xxxxxx.

675 **Reference**

- 676 Aldener, M., Brown, S. S., Stark, H., Williams, E. J., Lerner, B. M., Kuster, W. C., Goldan,
677 P. D., Quinn, P. K., Bates, T. S., Fehsenfeld, F. C., and Ravishankara, A. R.: Reactivity
678 and loss mechanisms of NO₃ and N₂O₅ in a polluted marine environment: Results
679 from in situ measurements during New England Air Quality Study 2002, *Journal of*
680 *Geophysical Research-Atmospheres*, 111, Artn D23s73, Doi 10.1029/2006jd007252,
681 2006.
- 682 Allan, B. J., Carslaw, N., Coe, H., Burgess, R. A., and Plane, J. M. C.: Observations of the
683 nitrate radical in the marine boundary layer, *Journal of Atmospheric Chemistry*, 33,
684 129-154, Doi 10.1023/A:1005917203307, 1999.
- 685 Atkinson, R., Baulch, D. L., Cox, R. A., Crowley, J. N., Hampson, R. F., Hynes, R. G.,
686 Jenkin, M. E., Rossi, M. J., and Troe, J.: Evaluated kinetic and photochemical data for
687 atmospheric chemistry: Volume I - gas phase reactions of O_x, HO_x, NO_x and SO_x
688 species, *Atmospheric Chemistry and Physics*, 4, 1461-1738, DOI 10.5194/acp-4-
689 1461-2004, 2004.
- 690 Ayres, B. R., Allen, H. M., Draper, D. C., Brown, S. S., Wild, R. J., Jimenez, J. L., Day, D.
691 A., Campuzano-Jost, P., Hu, W., de Gouw, J., Koss, A., Cohen, R. C., Duffey, K. C.,
692 Romer, P., Baumann, K., Edgerton, E., Takahama, S., Thornton, J. A., Lee, B. H.,

693 Lopez-Hilfiker, F. D., Mohr, C., Wennberg, P. O., Nguyen, T. B., Teng, A., Goldstein,
694 A. H., Olson, K., and Fry, J. L.: Organic nitrate aerosol formation via NO_3 + biogenic
695 volatile organic compounds in the southeastern United States, *Atmospheric Chemistry
696 and Physics*, 15, 13377-13392, 10.5194/acp-15-13377-2015, 2015.

697 Behnke, W., and, V., Scheer, and, C., and Zetzsch: 16 O 04 Formation of ClNO_2 and HNO_3
698 in the presence of N_2O_5 and wet pure NaCl- and wet mixed NaCl/ Na_2SO_4 - aerosol, *J
699 Aerosol Sci*, 24, S115-S116, 1993.

700 Bertram, T. H. and Thornton, J. A.: Toward a general parameterization of N_2O_5 reactivity
701 on aqueous particles: the competing effects of particle liquid water, nitrate and
702 chloride, *Atmospheric Chemistry and Physics*, 9, 8351-8363, 2009.

703 Brown, S. S. and Stutz, J.: Nighttime radical observations and chemistry, *Chem Soc Rev*,
704 41, 6405-6447, Doi 10.1039/C2cs35181a, 2012.

705 Brown, S. S., Stark, H., and Ravishankara, A. R.: Applicability of the steady state
706 approximation to the interpretation of atmospheric observations of NO_3 and N_2O_5 ,
707 *Journal of Geophysical Research-Atmospheres*, 108, Artn 4539, Doi
708 10.1029/2003jd003407, 2003.

709 Brown, S. S., Dube, W. P., Tham, Y. J., Zha, Q. Z., Xue, L. K., Poon, S., Wang, Z., Blake,
710 D. R., Tsui, W., Parrish, D. D., and Wang, T.: Nighttime chemistry at a high altitude
711 site above Hong Kong, *Journal of Geophysical Research-Atmospheres*, 121, 2457-
712 2475, 10.1002/2015jd024566, 2016.

713 Brown, S. S., Ryerson, T. B., Wollny, A. G., Brock, C. A., Peltier, R., Sullivan, A. P., Weber,
714 R. J., Dube, W. P., Trainer, M., Meagher, J. F., Fehsenfeld, F. C., and Ravishankara, A.
715 R.: Variability in nocturnal nitrogen oxide processing and its role in regional air quality,
716 *Science*, 311, 67-70, DOI 10.1126/science.1120120, 2006.

717 Brown, S. S., Dube, W. P., Peischl, J., Ryerson, T. B., Atlas, E., Warneke, C., de Gouw, J.
718 A., Hekkert, S. T., Brock, C. A., Flocke, F., Trainer, M., Parrish, D. D., Fehsenfeld, F.
719 C., and Ravishankara, A. R.: Budgets for nocturnal VOC oxidation by nitrate radicals
720 aloft during the 2006 Texas Air Quality Study, *Journal of Geophysical Research-
721 Atmospheres*, 116, Artn D24305, 10.1029/2011jd016544, 2011.

722 Brown, S. S., Dube, W. P., Fuchs, H., Ryerson, T. B., Wollny, A. G., Brock, C. A., Bahreini,
723 R., Middlebrook, A. M., Neuman, J. A., Atlas, E., Roberts, J. M., Osthoff, H. D.,
724 Trainer, M., Fehsenfeld, F. C., and Ravishankara, A. R.: Reactive uptake coefficients
725 for N_2O_5 determined from aircraft measurements during the Second Texas Air
726 Quality Study: Comparison to current model parameterizations, *Journal of
727 Geophysical Research-Atmospheres*, 114, Artn D00f10, 10.1029/2008jd011679, 2009.

728 Brown, S. S., Dube, W. P., Osthoff, H. D., Stutz, J., Ryerson, T. B., Wollny, A. G., Brock,
729 C. A., Warneke, C., De Gouw, J. A., Atlas, E., Neuman, J. A., Holloway, J. S., Lerner,
730 B. M., Williams, E. J., Kuster, W. C., Goldan, P. D., Angevine, W. M., Trainer, M.,
731 Fehsenfeld, F. C., and Ravishankara, A. R.: Vertical profiles in NO_3 and N_2O_5

732 measured from an aircraft: Results from the NOAA P-3 and surface platforms during
733 the New England Air Quality Study 2004, *Journal of Geophysical Research-*
734 *Atmospheres*, 112, Artn D22304, 10.1029/2007jd008883, 2007.

735 Brown, S. S., Dibb, J. E., Stark, H., Aldener, M., Vozella, M., Whitlow, S., Williams, E. J.,
736 Lerner, B. M., Jakoubek, R., Middlebrook, A. M., DeGouw, J. A., Warneke, C.,
737 Goldan, P. D., Kuster, W. C., Angevine, W. M., Sueper, D. T., Quinn, P. K., Bates, T.
738 S., Meagher, J. F., Fehsenfeld, F. C., and Ravishankara, A. R.: Nighttime removal of
739 NO_x in the summer marine boundary layer, *Geophysical Research Letters*, 31, Artn
740 L07108, Doi 10.1029/2004gl019412, 2004.

741 Chen, X., Wang, H., and Lu, K.: Interpretation of NO₃-N₂O₅ observation via steady state
742 in high-aerosol air mass: the impact of equilibrium coefficient in ambient conditions,
743 *Atmospheric Chemistry and Physics*, 22, 3525-3533, 10.5194/acp-22-3525-2022,
744 2022.

745 Chuang, M.-T., Chang, S.-C., Lin, N.-H., Wang, J.-L., Sheu, G.-R., Chang, Y.-J., and Lee,
746 C.-T.: Aerosol chemical properties and related pollutants measured in Dongsha Island
747 in the northern South China Sea during 7-SEAS/Dongsha Experiment, *Atmospheric*
748 *Environment*, 78, 82-92, 10.1016/j.atmosenv.2012.05.014, 2013.

749 Crowley, J. N., Thieser, J., Tang, M. J., Schuster, G., Bozem, H., Beygi, Z. H., Fischer, H.,
750 Diesch, J. M., Drewnick, F., Borrmann, S., Song, W., Yassaa, N., Williams, J., Pöhler,
751 D., Platt, U., and Lelieveld, J.: Variable lifetimes and loss mechanisms for NO₃ and
752 N₂O₅ during the DOMINO campaign: contrasts between marine, urban and
753 continental air, *Atmospheric Chemistry and Physics*, 11, 10853-10870, 10.5194/acp-
754 11-10853-2011, 2011.

755 Delhomme, O., Morville, S., and Millet, M.: Seasonal and diurnal variations of atmospheric
756 concentrations of phenols and nitrophenols measured in the Strasbourg area, France,
757 *Atmospheric Pollution Research*, 1, 16-22, 10.5094/apr.2010.003, 2010.

758 Dewald, P., Nussbaumer, C. M., Schuladen, J., Ringsdorf, A., Edtbauer, A., Fischer, H.,
759 Williams, J., Lelieveld, J., and Crowley, J. N.: Fate of the nitrate radical at the summit
760 of a semi-rural mountain site in Germany assessed with direct reactivity
761 measurements, *Atmospheric Chemistry and Physics*, 22, 7051-7069, 10.5194/acp-22-
762 7051-2022, 2022.

763 Edwards, P. M., Aikin, K. C., Dube, W. P., Fry, J. L., Gilman, J. B., de Gouw, J. A., Graus,
764 M. G., Hanisco, T. F., Holloway, J., Huber, G., Kaiser, J., Keutsch, F. N., Lerner, B.
765 M., Neuman, J. A., Parrish, D. D., Peischl, J., Pollack, I. B., Ravishankara, A. R.,
766 Roberts, J. M., Ryerson, T. B., Trainer, M., Veres, P. R., Wolfe, G. M., Warneke, C.,
767 and Brown, S. S.: Transition from high- to low-NO_x control of night-time oxidation
768 in the southeastern US, *Nat Geosci*, 10, 490+, 10.1038/Ngeo2976, 2017.

769 Evans, M. J. and Jacob, D. J.: Impact of new laboratory studies of N₂O₅ hydrolysis on
770 global model budgets of tropospheric nitrogen oxides, ozone, and OH, *Geophysical*

771 Research Letters, 32, Artn L09813, Doi 10.1029/2005gl022469, 2005.

772 Finlayson-Pitts, B. J., James N.: Chemistry of the upper and lower atmosphere: theory,
773 experiments and applications, Academic Press, Calif2000.

774 Fuentes., J. D., Lerdau., M., and Atkinson., R.:
775 Biogenic_hydrocarbons_in_the_atmospheric_Boundary_A review, B Am Meteorol
776 Soc, 2000.

777 Geyer, A., Alicke, B., Konrad, S., Schmitz, T., Stutz, J., and Platt, U.: Chemistry and
778 oxidation capacity of the nitrate radical in the continental boundary layer near Berlin,
779 Journal of Geophysical Research-Atmospheres, 106, 8013-8025, Doi
780 10.1029/2000jd900681, 2001.

781 Gu, S., Guenther, A., and Faiola, C.: Effects of Anthropogenic and Biogenic Volatile
782 Organic Compounds on Los Angeles Air Quality, Environ Sci Technol, 55, 12191-
783 12201, 10.1021/acs.est.1c01481, 2021.

784 Hallquist, M., Stewart, D. J., Stephenson, S. K., and Cox, R. A.: Hydrolysis of N₂O₅ on
785 sub-micron sulfate aerosols, Phys Chem Chem Phys, 5, 3453-3463, Doi
786 10.1039/B301827j, 2003.

787 Ian Barnes, Jens Hjorth, and Mihalopoulos, N.: Dimethyl Sulfide and Dimethyl Sulfoxide
788 and Their Oxidation in the Atmosphere, Chem Rev, 2006.

789 Kane, S. M., Caloz, F., and Leu, M. T.: Heterogeneous uptake of gaseous N₂O₅ by
790 (NH₄)₂SO₄, NH₄HSO₄, and H₂SO₄ aerosols, J Phys Chem A, 105, 6465-6470, Doi
791 10.1021/Jp010490x, 2001.

792 Kiendler-Scharr, A., Mensah, A. A., Friese, E., Topping, D., Nemitz, E., Prevot, A. S. H.,
793 Aijala, M., Allan, J., Canonaco, F., Canagaratna, M., Carbone, S., Crippa, M., Dall
794 Osto, M., Day, D. A., De Carlo, P., Di Marco, C. F., Elbern, H., Eriksson, A., Freney,
795 E., Hao, L., Herrmann, H., Hildebrandt, L., Hillamo, R., Jimenez, J. L., Laaksonen,
796 A., McFiggans, G., Mohr, C., O'Dowd, C., Otjes, R., Ovadnevaite, J., Pandis, S. N.,
797 Poulain, L., Schlag, P., Sellegri, K., Swietlicki, E., Tiitta, P., Vermeulen, A., Wahner,
798 A., Worsnop, D., and Wu, H. C.: Ubiquity of organic nitrates from nighttime chemistry
799 in the European submicron aerosol, Geophysical Research Letters, 43, 7735-7744,
800 10.1002/2016gl069239, 2016.

801 Li, Z., Xie, P., Hu, R., Wang, D., Jin, H., Chen, H., Lin, C., and Liu, W.: Observations of
802 N₂O₅ and NO₃ at a suburban environment in Yangtze river delta in China: Estimating
803 heterogeneous N₂O₅ uptake coefficients, J Environ Sci (China), 95, 248-255,
804 10.1016/j.jes.2020.04.041, 2020.

805 Liebmann, J., Karu, E., Sobanski, N., Schuladen, J., Ehn, M., Schallhart, S., Quelever, L.,
806 Hellen, H., Hakola, H., Hoffmann, T., Williams, J., Fischer, H., Lelieveld, J., and
807 Crowley, J. N.: Direct measurement of NO₃ radical reactivity in a boreal forest,
808 Atmospheric Chemistry and Physics, 18, 3799-3815, 10.5194/acp-18-3799-2018,
809 2018a.

810 Liebmann, J. M., Muller, J. B. A., Kubistin, D., Claude, A., Holla, R., Plass-Dulmer, C.,
811 Lelieveld, J., and Crowley, J. N.: Direct measurements of NO₃ reactivity in and above
812 the boundary layer of a mountaintop site: identification of reactive trace gases and
813 comparison with OH reactivity, *Atmospheric Chemistry and Physics*, 18, 12045-
814 12059, 10.5194/acp-18-12045-2018, 2018b.

815 Lin, C., Hu, R., Xie, P., Lou, S., Zhang, G., Tong, J., Liu, J., and Liu, W.: Nocturnal
816 atmospheric chemistry of NO₃ and N₂O₅ over Changzhou in the Yangtze River Delta
817 in China, *J Environ Sci (China)*, 114, 376-390, 10.1016/j.jes.2021.09.016, 2022.

818 Liu, X., Lyu, X., Wang, Y., Jiang, F., and Guo, H.: Intercomparison of O₃ formation and
819 radical chemistry in the past decade at a suburban site in Hong Kong, *Atmospheric
820 Chemistry and Physics*, 19, 5127-5145, 10.5194/acp-19-5127-2019, 2019.

821 Liu, X. G., Gu, J. W., Li, Y. P., Cheng, Y. F., Qu, Y., Han, T. T., Wang, J. L., Tian, H. Z.,
822 Chen, J., and Zhang, Y. H.: Increase of aerosol scattering by hygroscopic growth:
823 Observation, modeling, and implications on visibility, *Atmospheric Research*, 132,
824 91-101, 10.1016/j.atmosres.2013.04.007, 2013.

825 Lu, K. D., Zhang, Y. H., Su, H., Brauers, T., Chou, C. C., Hofzumahaus, A., Liu, S. C., Kita,
826 K., Kondo, Y., Shao, M., Wahner, A., Wang, J. L., Wang, X. S., and Zhu, T.: Oxidant
827 (O₃ + NO₂) production processes and formation regimes in Beijing, *Journal of
828 Geophysical Research-Atmospheres*, 115, Artn D07303, 10.1029/2009jd012714,
829 2010.

830 Lu, X., Qin, M., Xie, P., Duan, J., Fang, W., and Liu, W.: Observation of ambient NO₃
831 radicals by LP-DOAS at a rural site in North China Plain, *Sci Total Environ*, 804,
832 149680, 10.1016/j.scitotenv.2021.149680, 2022.

833 Lüttke, J., Scheer, V., Levsen, K., Wünsch, G., Cape, J. N., Hargreaves, K. J., Storeton-
834 West, R. L., Acker, K., Wieprecht, W., and Jones, B.: Occurrence and formation of
835 nitrated phenols in and out of cloud, *Atmospheric Environment*, 31, 2637-2648, 1997.

836 McMurry, P. H., Woo, K. S., Weber, R., Chen, D. R., and Pui, D. Y. H.: Size distributions
837 of 3-10 nm atmospheric particles: implications for nucleation mechanisms,
838 *Philosophical Transactions of the Royal Society a-Mathematical Physical and
839 Engineering Sciences*, 358, 2625-2642, 10.1098/rsta.2000.0673, 2000.

840 Mogensen, D., Gierens, R., Crowley, J. N., Keronen, P., Smolander, S., Sogachev, A.,
841 Nolscher, A. C., Zhou, L., Kulmala, M., Tang, M. J., Williams, J., and Boy, M.:
842 Simulations of atmospheric OH, O₃ and NO₃ reactivities within and above the boreal
843 forest, *Atmospheric Chemistry and Physics*, 15, 3909-3932, 10.5194/acp-15-3909-
844 2015, 2015.

845 Morgan, W. T., Ouyang, B., Allan, J. D., Aruffo, E., Di Carlo, P., Kennedy, O. J., Lowe, D.,
846 Flynn, M. J., Rosenberg, P. D., Williams, P. I., Jones, R., McFiggans, G. B., and Coe,
847 H.: Influence of aerosol chemical composition on N₂O₅ uptake: airborne regional
848 measurements in northwestern Europe, *Atmospheric Chemistry and Physics*, 15, 973-

849 990, DOI 10.5194/acp-15-973-2015, 2015.

850 Ng, N. L., Brown, S. S., Archibald, A. T., Atlas, E., Cohen, R. C., Crowley, J. N., Day, D.
851 A., Donahue, N. M., Fry, J. L., Fuchs, H., Griffin, R. J., Guzman, M. I., Herrmann, H.,
852 Hodzic, A., Iinuma, Y., Jimenez, J. L., Kiendler-Scharr, A., Lee, B. H., Luecken, D. J.,
853 Mao, J. Q., McLaren, R., Mutzel, A., Osthoff, H. D., Ouyang, B., Picquet-Varrault, B.,
854 Platt, U., Pye, H. O. T., Rudich, Y., Schwantes, R. H., Shiraiwa, M., Stutz, J., Thornton,
855 J. A., Tilgner, A., Williams, B. J., and Zaveri, R. A.: Nitrate radicals and biogenic
856 volatile organic compounds: oxidation, mechanisms, and organic aerosol,
857 Atmospheric Chemistry and Physics, 17, 2103-2162, 10.5194/acp-17-2103-2017,
858 2017.

859 Niu, Y. B., Zhu, B., He, L. Y., Wang, Z., Lin, X. Y., Tang, M. X., and Huang, X. F.: Fast
860 Nocturnal Heterogeneous Chemistry in a Coastal Background Atmosphere and Its
861 Implications for Daytime Photochemistry, Journal of Geophysical Research:
862 Atmospheres, 127, 10.1029/2022jd036716, 2022.

863 Osthoff, H. D., Pilling, M. J., Ravishankara, A. R., and Brown, S. S.: Temperature
864 dependence of the NO₃ absorption cross-section above 298 K and determination of
865 the equilibrium constant for NO₃ + NO₂ → N₂O₅ at atmospherically relevant
866 conditions, Phys Chem Chem Phys, 9, 5785-5793, 10.1039/b709193a, 2007.

867 Osthoff, H. D., Roberts, J. M., Ravishankara, A. R., Williams, E. J., Lerner, B. M.,
868 Sommariva, R., Bates, T. S., Coffman, D., Quinn, P. K., Dibb, J. E., Stark, H.,
869 Burkholder, J. B., Talukdar, R. K., Meagher, J., Fehsenfeld, F. C., and Brown, S. S.:
870 High levels of nitryl chloride in the polluted subtropical marine boundary layer, Nat
871 Geosci, 1, 324-328, Doi 10.1038/Ngeo177, 2008.

872 Riedel, T. P., Bertram, T. H., Crisp, T. A., Williams, E. J., Lerner, B. M., Vlasenko, A., Li,
873 S. M., Gilman, J., de Gouw, J., Bon, D. M., Wagner, N. L., Brown, S. S., and Thornton,
874 J. A.: Nitryl Chloride and Molecular Chlorine in the Coastal Marine Boundary Layer,
875 Environmental Science & Technology, 46, 10463-10470, 10.1021/es204632r, 2012.

876 Riedel, T. P., Wolfe, G. M., Danas, K. T., Gilman, J. B., Kuster, W. C., Bon, D. M., Vlasenko,
877 A., Li, S. M., Williams, E. J., Lerner, B. M., Veres, P. R., Roberts, J. M., Holloway, J.
878 S., Lefer, B., Brown, S. S., and Thornton, J. A.: An MCM modeling study of nitryl
879 chloride (ClNO₂) impacts on oxidation, ozone production and nitrogen oxide
880 partitioning in polluted continental outflow, Atmospheric Chemistry and Physics, 14,
881 3789-3800, 10.5194/acp-14-3789-2014, 2014.

882 Rosati, B., Isokääntä, S., Christiansen, S., Jensen, M. M., Moosakutty, S. P., Wollesen de
883 Jonge, R., Massling, A., Glasius, M., Elm, J., Virtanen, A., and Bilde, M.:
884 Hygroscopicity and CCN potential of DMS-derived aerosol particles, Atmospheric
885 Chemistry and Physics, 22, 13449-13466, 10.5194/acp-22-13449-2022, 2022.

886 Tang, M. J., Schuster, G., and Crowley, J. N.: Heterogeneous reaction of N₂O₅ with illite
887 and Arizona test dust particles, Atmospheric Chemistry and Physics, 14, 245-254,

888 DOI 10.5194/acp-14-245-2014, 2014.

889 Tham, Y. J., Wang, Z., Li, Q., Wang, W., Wang, X., Lu, K., Ma, N., Yan, C., Kecorius, S.,
890 Wiedensohler, A., Zhang, Y., and Wang, T.: Heterogeneous N₂O₅ uptake coefficient
891 and production yield of ClNO₂ in polluted northern China: roles of aerosol water
892 content and chemical composition, *Atmos. Chem. Phys.*, 18, 13155-13171,
893 10.5194/acp-18-13155-2018, 2018.

894 Tham, Y. J., Wang, Z., Li, Q. Y., Yun, H., Wang, W. H., Wang, X. F., Xue, L. K., Lu, K. D.,
895 Ma, N., Bohn, B., Li, X., Kecorius, S., Gross, J., Shao, M., Wiedensohler, A., Zhang,
896 Y. H., and Wang, T.: Significant concentrations of nitryl chloride sustained in the
897 morning: investigations of the causes and impacts on ozone production in a polluted
898 region of northern China, *Atmospheric Chemistry and Physics*, 16, 14959-14977,
899 10.5194/acp-16-14959-2016, 2016.

900 Thornton, J. A., Kercher, J. P., Rie De L, T. P., Wagner, N. L., Cozic, J., Holloway, J. S.,
901 Dubé, W., Wolfe, G. M., Quinn, P. K., and Middlebrook, A. M.: A large atomic
902 chlorine source inferred from mid-continental reactive nitrogen chemistry, *Nature*,
903 464, 271-274, 2010.

904 Vrekoussis, M., Mihalopoulos, N., Gerasopoulos, E., Kanakidou, M., Crutzen, P. J., and
905 Lelieveld, J.: Two-years of NO₃ radical observations in the boundary layer over the
906 Eastern Mediterranean, *Atmospheric Chemistry and Physics*, 7, 315-327, 2007.

907 Vrekoussis, M., Kanakidou, M., Mihalopoulos, N., Crutzen, P. J., Lelieveld, J., Perner, D.,
908 Berresheim, H., and Baboukas, E.: Role of the NO₃ radicals in oxidation processes in
909 the eastern Mediterranean troposphere during the MINOS campaign, *Atmospheric
910 Chemistry and Physics*, 4, 169-182, 2004.

911 Wagner, N. L., Riedel, T. P., Young, C. J., Bahreini, R., Brock, C. A., Dube, W. P., Kim, S.,
912 Middlebrook, A. M., Ozturk, F., Roberts, J. M., Russo, R., Sive, B., Swarthout, R.,
913 Thornton, J. A., VandenBoer, T. C., Zhou, Y., and Brown, S. S.: N₂O₅ uptake
914 coefficients and nocturnal NO₂ removal rates determined from ambient wintertime
915 measurements, *Journal of Geophysical Research-Atmospheres*, 118, 9331-9350, Doi
916 10.1002/Jgrd.50653, 2013.

917 Wang, H., Chen, J., and Lu, K.: Development of a portable cavity-enhanced absorption
918 spectrometer for the measurement of ambient NO₃ and N₂O₅: experimental setup, lab
919 characterizations, and field applications in a polluted urban environment, *Atmos Meas
920 Tech*, 10, 1465-1479, 10.5194/amt-10-1465-2017, 2017a.

921 Wang, H., Chen, T., and Lu, K.: Measurement of NO₃ and N₂O₅ in the Troposphere,
922 *Progress in Chemistry*, 27, 963-976, 10.7536/pc141230, 2015.

923 Wang, H., Lu, K., Chen, S., Li, X., Zeng, L., Hu, M., and Zhang, Y.: Characterizing nitrate
924 radical budget trends in Beijing during 2013–2019, *Science of The Total Environment*,
925 795, 10.1016/j.scitotenv.2021.148869, 2021.

926 Wang, H., Wang, H., Lu, X., Lu, K., Zhang, L., Tham, Y. J., Shi, Z., Aikin, K., Fan, S.,

927 Brown, S. S., and Zhang, Y.: Increased night-time oxidation over China despite
928 widespread decrease across the globe, *Nat Geosci*, 10.1038/s41561-022-01122-x,
929 2023.

930 Wang, H., Lyu, X., Guo, H., Wang, Y., Zou, S., Ling, Z., Wang, X., Jiang, F., Zeren, Y., Pan,
931 W., Huang, X., and Shen, J.: WS-Ozone pollution around a coastal region of South
932 China Sea: interaction between marine and continental air, *Atmospheric Chemistry
933 and Physics*, 18, 4277-4295, 10.5194/acp-18-4277-2018, 2018a.

934 Wang, H., Chen, X., Lu, K., Hu, R., Li, Z., Wang, H., Ma, X., Yang, X., Chen, S., Dong,
935 H., Liu, Y., Fang, X., Zeng, L., Hu, M., and Zhang, Y.: NO₃ and N₂O₅ chemistry at a
936 suburban site during the EXPLORE-YRD campaign in 2018, *Atmospheric
937 Environment*, 224, 10.1016/j.atmosenv.2019.117180, 2020a.

938 Wang, H., Chen, X., Lu, K., Tan, Z., Ma, X., Wu, Z., Li, X., Liu, Y., Shang, D., Wu, Y.,
939 Zeng, L., Hu, M., Schmitt, S., Kiendler-Scharr, A., Wahner, A., and Zhang, Y.:
940 Wintertime N₂O₅ uptake coefficients over the North China Plain, *Science Bulletin*, 65,
941 765-774, 10.1016/j.scib.2020.02.006, 2020b.

942 Wang, H., Lu, K., Guo, S., Wu, Z., Shang, D., Tan, Z., Wang, Y., Le Breton, M., Lou, S.,
943 Tang, M., Wu, Y., Zhu, W., Zheng, J., Zeng, L., Hallquist, M., Hu, M., and Zhang, Y.:
944 Efficient N₂O₅ uptake and NO₃ oxidation in the outflow of urban Beijing,
945 *Atmospheric Chemistry and Physics*, 18, 9705-9721, 10.5194/acp-18-9705-2018,
946 2018b.

947 Wang, H., Lu, K., Chen, X., Zhu, Q., Chen, Q., Guo, S., Jiang, M., Li, X., Shang, D., Tan,
948 Z., Wu, Y., Wu, Z., Zou, Q., Zheng, Y., Zeng, L., Zhu, T., Hu, M., and Zhang, Y.: High
949 N₂O₅ Concentrations Observed in Urban Beijing: Implications of a Large Nitrate
950 Formation Pathway, *Environmental Science & Technology Letters*, 4, 416-420,
951 10.1021/acs.estlett.7b00341, 2017b.

952 Wang, H., Yuan, B., Zheng, E., Zhang, X., Wang, J., Lu, K., Ye, C., Yang, L., Huang, S.,
953 Hu, W., Yang, S., Peng, Y., Qi, J., Wang, S., He, X., Chen, Y., Li, T., Wang, W.,
954 Huangfu, Y., Li, X., Cai, M., Wang, X., and Shao, M.: Formation and impacts of nitryl
955 chloride in Pearl River Delta, *Atmospheric Chemistry and Physics*, 22, 14837-14858,
956 10.5194/acp-22-14837-2022, 2022.

957 Wang, S. S., Shi, C. Z., Zhou, B., Zhao, H., Wang, Z. R., Yang, S. N., and Chen, L. M.:
958 Observation of NO₃ radicals over Shanghai, China, *Atmospheric Environment*, 70,
959 401-409, DOI 10.1016/j.atmosenv.2013.01.022, 2013.

960 Wang, X. F., Wang, H., Xue, L. K., Wang, T., Wang, L. W., Gu, R. R., Wang, W. H., Tham,
961 Y. J., Wang, Z., Yang, L. X., Chen, J. M., and Wang, W. X.: Observations of N₂O₅ and
962 ClNO₂ at a polluted urban surface site in North China: High N₂O₅ uptake coefficients
963 and low ClNO₂ product yields, *Atmospheric Environment*, 156, 125-134,
964 10.1016/j.atmosenv.2017.02.035, 2017c.

965 Wang, Z., Wang, W. H., Tham, Y. J., Li, Q. Y., Wang, H., Wen, L., Wang, X. F., and Wang,

966 T.: Fast heterogeneous N_2O_5 uptake and ClNO_2 production in power plant and
 967 industrial plumes observed in the nocturnal residual layer over the North China Plain,
 968 Atmospheric Chemistry and Physics, 17, 12361-12378, 10.5194/acp-17-12361-2017,
 969 2017d.

970 Wang, J., Wang, H., Tham, Y. J., Ming, L., Zheng, Z., Fang, G., Sun, C., Ling, Z., Zhao, J.,
 971 and Fan, S.. (2023). Measurement report: Atmospheric nitrate radical chemistry in the
 972 South China Sea influenced by the urban outflow of the Pearl River Delta [Data set].
 973 Zenodo. <https://doi.org/10.5281/zenodo.8089100>.

974 Wayne, R. P., Barnes, I., Biggs, P., Burrows, J. P., Canosamas, C. E., Hjorth, J., Lebras, G.,
 975 Moortgat, G. K., Perner, D., Poulet, G., Restelli, G., and Sidebottom, H.: The Nitrate
 976 Radical - Physics, Chemistry, and the Atmosphere, Atmos Environ a-Gen, 25, 1-203,
 977 Doi 10.1016/0960-1686(91)90192-A, 1991.

978 Wood, E. C., Bertram, T. H., Wooldridge, P. J., and Cohen, R. C.: Measurements of N_2O_5 ,
 979 NO_2 , and O_3 east of the San Francisco Bay, 2005.

980 Xu, L., Guo, H., Boyd, C. M., Klein, M., Bougiatioti, A., Cerully, K. M., Hite, J. R.,
 981 Isaacman-VanWertz, G., Kreisberg, N. M., Knote, C., Olson, K., Koss, A., Goldstein,
 982 A. H., Hering, S. V., de Gouw, J., Baumann, K., Lee, S. H., Nenes, A., Weber, R. J.,
 983 and Ng, N. L.: Effects of anthropogenic emissions on aerosol formation from isoprene
 984 and monoterpenes in the southeastern United States (vol 112, pg 37, 2015), P Natl
 985 Acad Sci USA, 112, E4506-E4507, 2015.

986 Yan, C., Tham, Y. J., Zha, Q. Z., Wang, X. F., Xue, L. K., Dai, J. N., Wang, Z., and Wang,
 987 T.: Fast heterogeneous loss of N_2O_5 leads to significant nighttime NO_x removal and
 988 nitrate aerosol formation at a coastal background environment of southern China,
 989 Science of the Total Environment, 677, 637-647, 10.1016/j.scitotenv.2019.04.389,
 990 2019.

991 Yan, Y., Wang, S., Zhu, J., Guo, Y., Tang, G., Liu, B., An, X., Wang, Y., and Zhou, B.:
 992 Vertically increased NO_3 radical in the nocturnal boundary layer, Sci Total Environ,
 993 763, 142969, 10.1016/j.scitotenv.2020.142969, 2021.

994 Yang, S., Yuan, B., Peng, Y., Huang, S., Chen, W., Hu, W., Pei, C., Zhou, J., Parrish, D. D.,
 995 Wang, W., He, X., Cheng, C., Li, X.-B., Yang, X., Song, Y., Wang, H., Qi, J., Wang,
 996 B., Wang, C., Wang, C., Wang, Z., Li, T., Zheng, E., Wang, S., Wu, C., Cai, M., Ye,
 997 C., Song, W., Cheng, P., Chen, D., Wang, X., Zhang, Z., Wang, X., Zheng, J., and Shao,
 998 M.: The formation and mitigation of nitrate pollution: comparison between urban and
 999 suburban environments, Atmospheric Chemistry and Physics, 22, 4539-4556,
 1000 10.5194/acp-22-4539-2022, 2022.

1001 Yu, C., Wang, Z., Xia, M., Fu, X., Wang, W., Tham, Y. J., Chen, T., Zheng, P., Li, H., Shan,
 1002 Y., Wang, X., Xue, L., Zhou, Y., Yue, D., Ou, Y., Gao, J., Lu, K., Brown, S. S., Zhang,
 1003 Y., and Wang, T.: Heterogeneous N_2O_5 reactions on atmospheric aerosols at four
 1004 Chinese sites: improving model representation of uptake parameters, Atmos. Chem.

1005 Phys., 20, 4367-4378, 10.5194/acp-20-4367-2020, 2020.

1006 Yun, H., Wang, T., Wang, W. H., Tham, Y. J., Li, Q. Y., Wang, Z., and Poon, S. C. N.:
1007 Nighttime NO_x loss and ClNO₂ formation in the residual layer of a polluted region:
1008 Insights from field measurements and an iterative box model, *Science of the Total*
1009 *Environment*, 622, 727-734, 10.1016/j.scitotenv.2017.11.352, 2018a.

1010 Yun, H., Wang, W. H., Wang, T., Xia, M., Yu, C., Wang, Z., Poon, S. C. N., Yue, D. L., and
1011 Zhou, Y.: Nitrate formation from heterogeneous uptake of dinitrogen pentoxide during
1012 a severe winter haze in southern China, *Atmospheric Chemistry and Physics*, 18,
1013 17515-17527, 10.5194/acp-18-17515-2018, 2018b.

1014 Zhou, W., Zhao, J., Ouyang, B., Mehra, A., Xu, W. Q., Wang, Y. Y., Bannan, T. J., Worrall,
1015 S. D., Priestley, M., Bacak, A., Chen, Q., Xie, C. H., Wang, Q. Q., Wang, J. F., Du, W.,
1016 Zhang, Y. J., Ge, X. L., Ye, P. L., Lee, J. D., Fu, P. Q., Wang, Z. F., Worsnop, D., Jones,
1017 R., Percival, C. J., Coe, H., and Sun, Y. L.: Production of N₂O₅ and ClNO₂ in summer
1018 in urban Beijing, China, *Atmospheric Chemistry and Physics*, 18, 11581-11597,
1019 10.5194/acp-18-11581-2018, 2018.

1020 Zhu, J., Wang, S., Zhang, S., Xue, R., Gu, C., and Zhou, B.: Changes in NO₃ Radical and
1021 Its Nocturnal Chemistry in Shanghai From 2014 to 2021 Revealed by Long - Term
1022 Observation and a Stacking Model: Impact of China's Clean Air Action Plan, *Journal*
1023 *of Geophysical Research: Atmospheres*, 127, 10.1029/2022jd037438, 2022.

1024